Optimal Deposition Conditions of TiN Barrier Layers for the Growth of Vertically Aligned Carbon Nanofibers

Damon Rafieian

Department of Microtechnology and Nanoscience
Division of BioNano Systems Laboratory
CHALMERS UNIVERSITY OF TECHNOLOGY
Göteborg, Sweden 2010

Optimal Deposition Conditions of TiN Barrier Layers for the Growth of Vertically Aligned Carbon Nanofibers

Optimal Deposition Conditions of TiN Barrier Layers for the Growth of Vertically Aligned Carbon Nanofibers
Master's Thesis in the Master's programme in Microtechnology
DAMON RAFIEIAN
Department of Microtechnology and Nanoscience
Division of BioNano Systems Laboratory
Chalmers University of Technology

Abstract

The synthesis of vertically aligned carbon nanofibers (VACNF) employing catalytic plasma enhanced chemical vapor deposition has rendered them a distinguished building block for the fabrication of nano-electromechanical devices (NEMS). However, it is clear that the electrical properties of such a device are highly affected by the electrical properties of the underlying material. Nevertheless, the existing excellent candidates such as gold and copper must be isolated from the catalyst material by a diffusion barrier layer in order to hinder the interdiffusion while good electrical contact to the nanofibers is maintained. Being known as a good diffusion barrier with relatively low resistivity, TiN has been nominated to serve the purpose. On the other hand, depending on the deposition condition, the microstructure and resulting TiN properties varies to a large extent. In this work we have developed a novel method to deposit stoichiometric TiN using dc reactive magnetron sputtering and evaluated the diffusion barrier of the sputtered TiN film continuously by annealing them in a plasma enhanced chemical vapor deposition (PECVD) chamber. Furthermore, we have successfully minimized the resistivity of the sputtered TiN by modification of the sputtering conditions. We have employed an easy-to-implement, high throughput and inexpensive technique called colloidal lithography for patterning the Ni catalysts dots on top of the TiN substrates. The composition ratio and transition between the phases of sputtered TiN films have been characterized by X-ray photoelectron spectroscopy as well.

Keywords: Vertically aligned carbon nanofibers, Titanium Nitride, Diffusion, dc reactive sputtering, Four-point-probe resistivity measurement, Nanoelectromechanical systems

List of Appended Papers

A **The Impacts of Ti-N Film Properties on the Synthesis Of Vertically Aligned Carbonnanofibers:Presented in carbon 2010 conference held at Clemson University**

Farzan A. Ghavanini, Maria L. Damian, Damon Rafieian and Per Lundgren

B **Growth characterization of vertically aligned carbon nanofibers on top of TiN buffer layer for nanoelectromechanical devices:Presented in eurosensor 2010 conference held at Linz,Austria**

Farzan A. Ghavanini , Maria E. L. Damian, Damon Rafieian, and Per Lundgren

C **Characterization of vertically aligned carbon nanofiber growth on top of optimized TiN diffusion barrier layers:Presented in micronano system worshop conference held at Stockholm,Sweden**

Farzan A. Ghavanini, Maria Lopez-Damian1, Damon Rafieian, Krister Svensson, Per Lundgren, and Peter Enoksson

Contents

Acknowledgements

First all I have to express my gratitude to my supervisor Farzan Alavian Ghavanini for his guidance,support and advice from the initial to final level. Without his contribution this work would not have been possible.

I am grateful to my examiner Per Lundgren for reviewing my thesis accurately and giving his beneficial advice and corrections.

I would like to thank Henrik Frederiksen,Mahdad Sadeghi and Orjan Arthursson for assisting me with cleanroom processings.

I am indebted to Peter Enoksson,Anke Sanz-Velasco and all BNSL colleagues for their countless scientific discussions.

I would like to thank Nabi Nabiollahi for his contribution to graphical illustrations within this work.

My deepest gratitiude belongs to my family for being patient, supportive and motivating during my studies.

1 Introduction

The growing need for miniaturization and integration has brought about a fierce competition for introducing novel materials to microelectronic industry. Carbon nanotubes (CNT) and carbon nano fibers (CNF), two important allotropes of carbon [1] are among the materials proposed by ITRS [1] as the viable alternatives for reducing the adverse effect of miniaturization. The ability to withstand a current density up to and the highest Young's modulus [2]compared to other materials are just a few appealing CNT properties to mention. Although these outstanding properties are attributed to these carbon base structures, there is still a long way to employ them in electronic devices for several reasons. The reproducibility, controllability and consistency in quality of CNTs are prominent roadblocks to employ them as CNT based electronic devices. For instance, it is still challenging to obtain purely conductive CNTs due to the link between the chirality of graphene sheets as their building blocks and conductivity. Statistically, only one third of the CNTs are only metallic [3]and this makes them useless when conductivity is indispensable such as carbon base naoelectromechanical (NEMS) devices. Vertical alignment is another requirement that must be fulfilled in certain applications. Vertical alignment in places with high density of CNT is only obtained by van der Waals force between the individual tubes [4]indicating that single vertically aligned CNT could only be achieved by complicated post synthesis processes. CNFs in comparison to CNTs have not perfect cylindrical atomic structure but instead due to their structure they are always conductive and in some synthesis circumstances could be vertically aligned without relying on local van der Waals forces. These two appealing characteristics add more weight to realization of a carbonnanofiber based nanoelectromechanical device functioning as a variable capacitor (Figure 1.1).

1.1 Objectives

This work is part of a project aiming to fabricate a carbon nanofiber base naoelectromechanical device functioning as a variable capacitor (varactor). We have employed catalytic plasma enhanced chemical vapour deposition (c-PECVD) as the vertically aligned carbon nanofibers (VANCFs) synthesis method and TiN as the underlayer (Figure 1.2) on which they are grown. TiN has been nominated for this pupose due to its complementary metal-oxide-semiconductor (CMOS) compatibility, diffusion barrier performance, good conductivity and popularity among the research community. Thanks to the method of growth for the selected CNFs all of the requirements for our device including vertical alignment, diameter controllability and determined position have been met. The main focus of this thesis is an attempt to optimize the reactive sputtering condition of TiN as the underlayer leading to high quality TiN in terms of minimum diffusion and minimum resistivity. At the starting point of the project we encountered the disappearance of 10 nm-thick nickel catalyst seeds after the annealing step. This hindered the free standing nanofibers growth obliging us to apply thicker catalyst seeds (50 nm) which is

---

[1]The International Technology Roadmap for Semiconductors (ITRS) is an assessment of the semiconductor industry's technology requirements.

(a) Single pair   (b) Array
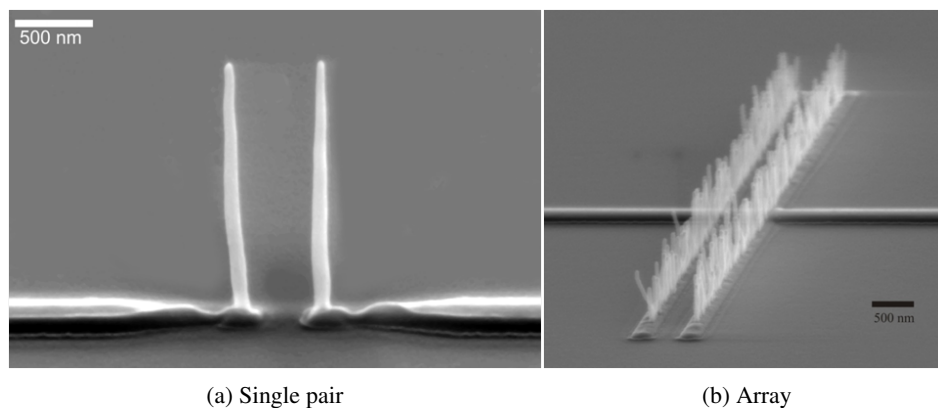
Figure 1.1: SEM micrographs of single pair of VACNF based device (Left) and an array of VACNFs functioning as a variable capacitor (right)

not favorable. This adverse phenomenon is attributed to diffusion of nickel into a defective TiN film which also displays high electrical resistivity. This motivates us to run several series of experimental trials under various conditions to find the remedy. Two different dc magnetron sputtering systems with different reactor geometry were employed and several assessments techniques such as four-point probe resistivity measurement, X-ray photoelectron spectroscopy and scanning electron microscopy were used to investigate the quality of the film.

Figure 1.2: Schematic illustration and corresponding SEM micrograph of VACNFs substrate's layers

2 Background

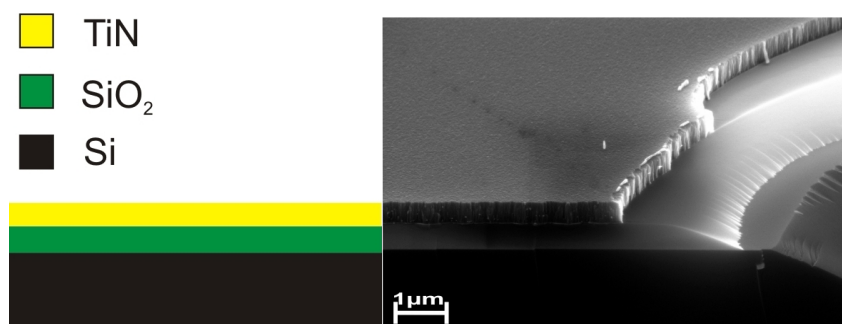## 2.1 Carbon nanotubes

The discovery of carbon nanotubes is still a controversial issue but the majority of science and technology journalsattributed it to Suomo Iijima, a scientist at NEC Japan [5]. The elementary form of CNTs consists of one sheet of graphene wrapped in cylindrical geometry which is called a single-wall carbon nanotubes(SWCNT). The electrical properties of CNTs lie at the wrapping direction of graphene along the cylindrical axis known as chirality. Based on the chirality they are classified as either zigzag, armchair or chiral with varying electrical properties (Figure 2.1). The chiral vector (Figure 2.1(d)) is
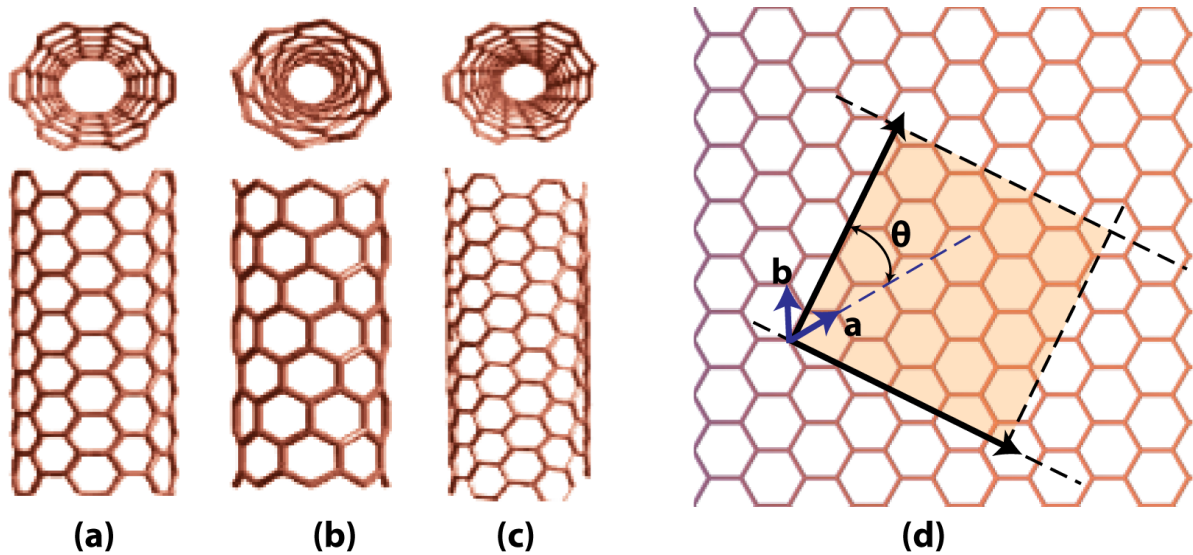

Figure 2.1: (a) Armchair, (b) Zigzag , (c) Chiral Carbon nanotubes and (d)a layer of graphene sheet

defined as $C_h=na_1+ma_2$ where n and m plays a prominent role in determining the electrical properties of SWCNT. CNTs can be consisted of more than one graphene layer and in that case they are called multi-wall carbon nanotubes (MWCNT). The number of walls varies from two up to a few tens.

Structures that extend perpendicularly from the substrate on which they are grown called vertically aligned. Vertical alignment, which is a prerequisite for our carbon base NEMS device, can be achieved either in dense forests through van der Waals forces between nanotubes or through the interaction of growing nanofibers with an electric field [4]. There are also some post synthesis techniques in order to have individual vertically aligned CNTs which are quite expensive and time consuming. For instance, Teng et al employed a method to grow CNTs vertically in silicon vias (Figure 2.2). Melchko et al. reported also using a nanoporous template for vertical alignment[4].
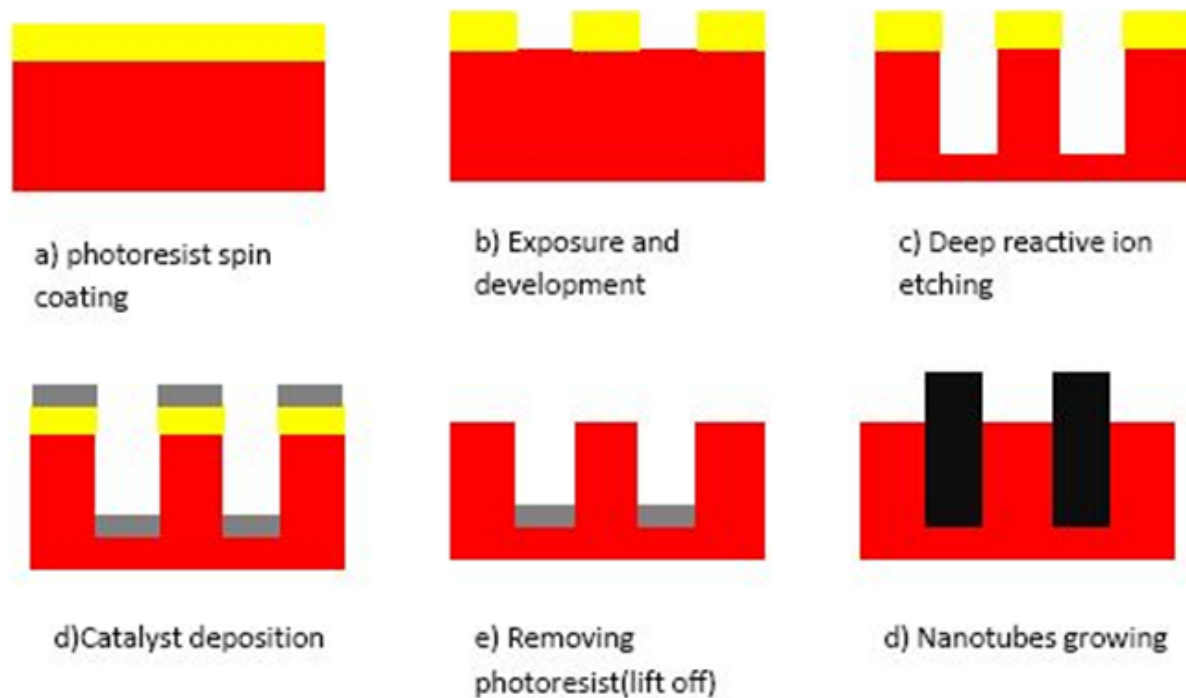
Figure 2.2: The schematic illustration of growing CNTs in silicon vias

2.2 Carbon nanofibers

Carbon nanofibers (CNF) are one of the main allotropes of carbon. They are cylindrical or conical structures with high aspect ratio. CNFs consist of curved graphite layer placed on top of each other producing two main configurations; herringbone and bamboo type (Figure 2.3(b,c)). There is a link between CNT and CNF based on the angle between the fiber axis and the graphene layers denoted by α (Figure 2.3). When α=0 the resultant nanostructure is called CNTs possessing outstanding electrical and mechanical properties. As the angle becomes larger than zero the properties of the resultant CNF undergoes huge difference due to the emergence of interplane components (Figure 2.3). From electrical point of view, charge transport along the fibers takes an interplane path in addition to occuring inplane. The same applies to mechanical properties where the van der Waals bonding between the graphene layers differs from the covalent bonding within the planes which degrades their stiffness compared to CNTs.

Among the different CNF synthesis methods such as arc discharge, laser ablation, and certain types of chemical vapor deposition, catalytic plasma enhanced chemical vapor deposition (c-PECVD) gives fibers with desirable alignment due to the interaction of growing fibers with the electrical field induced by the plasma inside CVD chamber. In general, the c-PECVD method includes three consecutive steps; pretreatment or annealing in which the final temperature and its ramp rate is controlled while an etchant gas is introduced into the chamber, plasma treatment and finally the growth of fibers by adding a precursors gas . The disappearance of nickel catalyst occurs at the annealing step where TiN and nickel catalyst dots are exposed to elevated temperatures with different ramp rates. The annealing step is deemed in our work as a reasonable bench mark for assessing the diffusion barrier performance of TiN produced under different sputtering conditions.
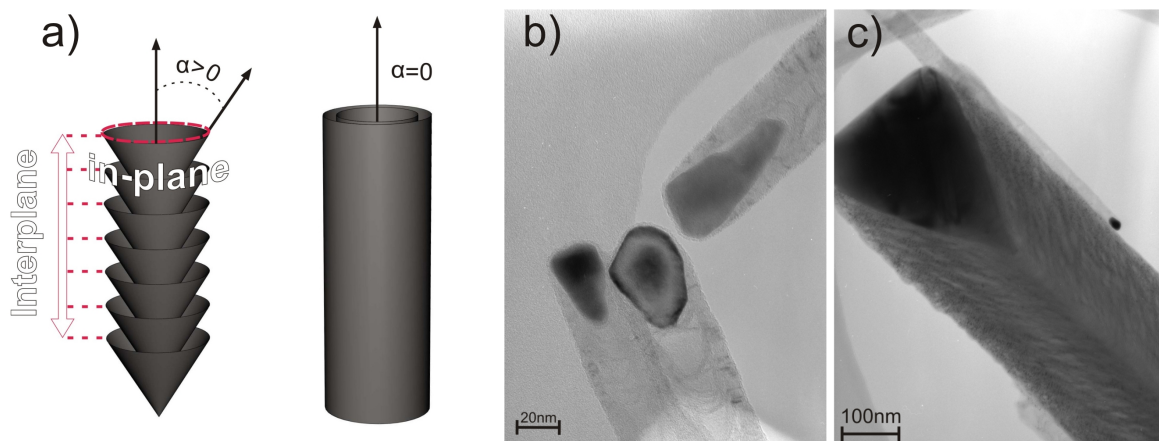
Figure 2.3: A schematic illustrations of Carbon Nanofibers and Multwalled Carbon Nanotubes (a) A SEM micrograph of bamboo type CNF(B) and herringbone CNF(c)

2.3 Titanium nitride (TiN) thin-film

Nitrogen can be incorporated in many compounds such as N_2O or NCl_3 but the term nitride is only used when nitrogen appears in a compound with an element with equal or lower electronegativity. With respect to the electronic structure and bonding condition, TiN is classified as an interstitial nitride where nitrogen atoms lie in the interstices of the titanium lattice sites (octahederal sites)[1] giving a closed packed crystalline structure. Due to the covalent bonds between the elements, it has a good electrical and thermal conductivity. The crystalline structure and as a consequence, the physical properties of TiN vary depending on the amount of incorporated nitrogen as result of defective filling of available sites. Based on the nitrogen content in the film the crystal structure changes as follows:

For films containing less than 15 at.% N only single phase α-Ti structure appears while films with nitrogen content more than 15 at.% N has tetragonal ε-Ti_2N structure. As the film approaches the stoichiometric state, single phase δTiN is observed (Figure 2.4)[6]. Stoichiometric TiN gives maximum density with the highest diffusion barrier performance, the highest hardness and minimum electrical resistivity [7]. It is also widely reported that by increasing the nitrogen content in the film the color of the film changes from metallic grey in the so-called titanium rich area, to goldish in the stoichiometric region and finally reaches to dark brownish in the nitrogen rich case[8]. Cross-sectional transmission electron microscopy revealed the presence of grains with diameter about 0.02 μm (for a film 0.1 μm in thickness)[9]. It is also reported that the oxygen content in the film varies from less than 1 at.% for substoichiometric film to about 4 at.% for hyperstoichiometric films[9]. TiN applications in semiconductor industry are divided into three main groups; diffusion barrier in silicon metallization, contact layer for silicon and a feasible alternative for gate electrode in very large scale metal oxide semiconductor integrated circuits[10]. It has also been reported due to the low concentration of contaminating alkali-elements metals it is a promising alternative for ideal metal-oxide-semiconductor capacitors[9].

The TiN film growth originates from the formation of nuclei or clusters consisting of absorbed species

---

[1]There are two different sites inside the metal lattice; octahedral and tetrahedral. Tetrahedral sites are too small to accommodate nitrogen.
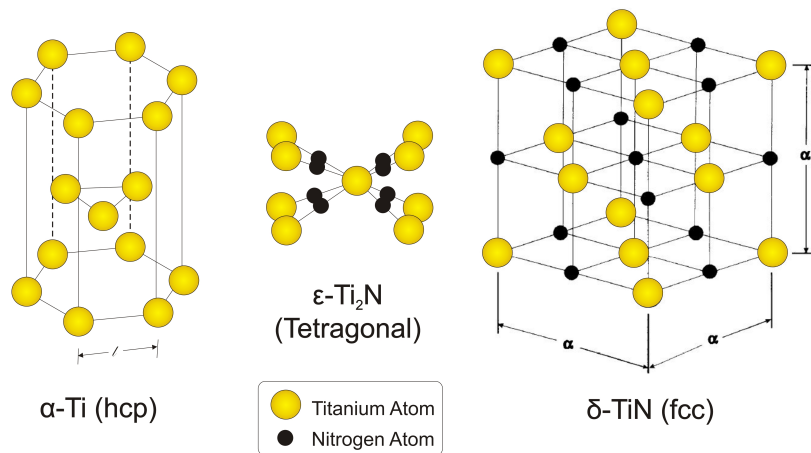
Figure 2.4: Different phases and Crystal structures of TiN

on the substrate. These nuclei grow either along the substrate or perpendicular to it producing islands. Regardless of the thermodynamics and kinetics of deposition almost all film growth starts from island formation. After the continuous film is formed the growth proceeds normal to the substrate in columnar structure (Figure 2.5).
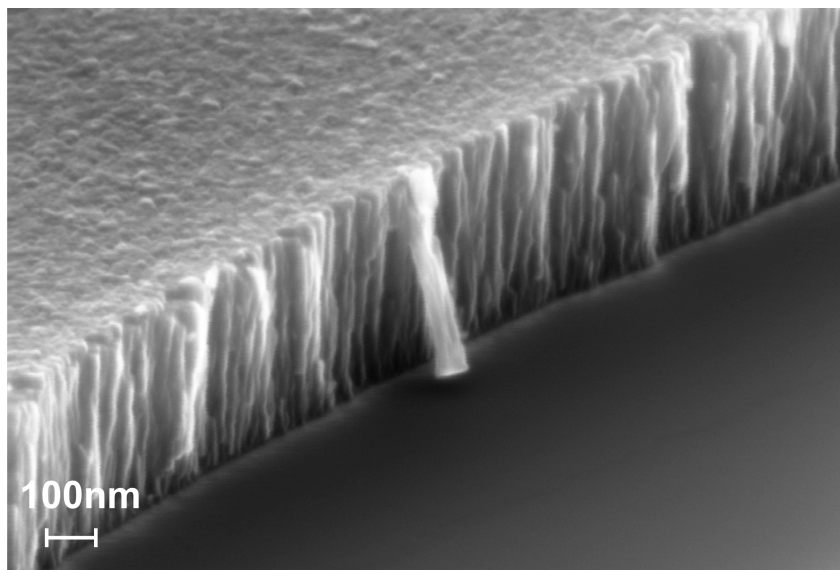
Figure 2.5: A SEM micrograph of a reactively sputtered Tin. The columnar structure is clearly seen

It is reported that regardless of the type of material and method of deposition the structure of the growing film is columnar[11].

Deposition conditions have a pronounced effect on the microstructure and stoichiometry of the film which in turn can affect the resistivity, density and diffusion properties of the resulting film. Thus, in order to produce TiN with good diffusion barrier performance and minimum resistivity and also reproducibility it is imperative to have a good control over deposition parameters for the employed equipment.

2.4 Methods

2.4.1 Basic sputtering configuration(DIODE)

The sputtering phenomenon is defined as the separation of atoms from the surface of specific solid material called the source or the target, through its bombardment by the energetic ions inside a reduced pressure ambient. As these ejected atoms reach the substrate they lose their momentum and form a thin film atomistically. The primary configuration of the so-called diode sputtering is schematically shown in (Figure 2.6. A glow discharge or plasma is formed between two electrodes positioned in parallel. The
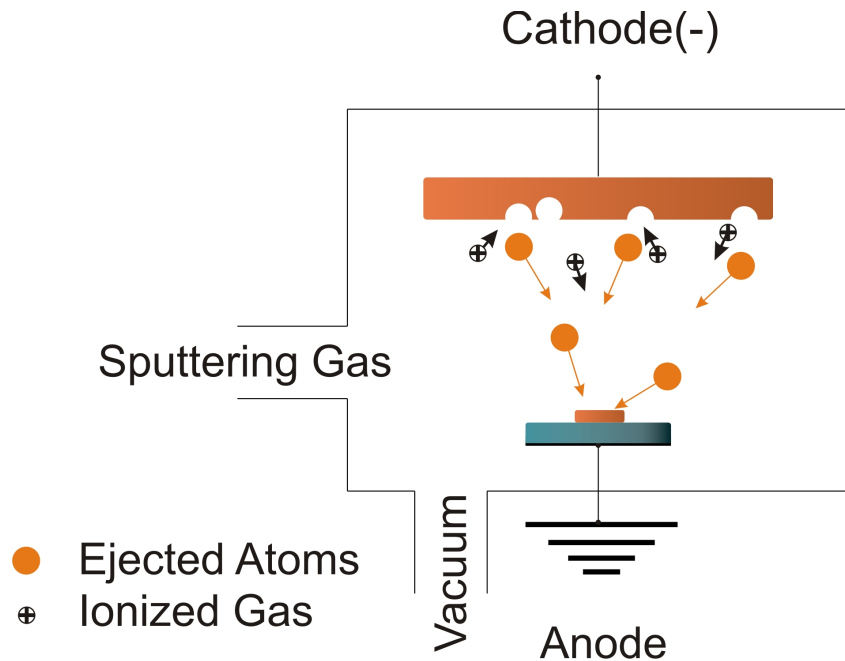

Figure 2.6: A schematic illustration of the diode sputtering

cathode (-) is connected to a power supply which could be either DC or RF, and the anode is connected to the substrate which could be biased negatively or positively, grounded, heated or combination of these parameters based on the requirement of the thin film. Firstly the chamber is evacuated then the sputtering gas which is typically argon is introduced to the chamber. The pressure inside the chamber usually ranges from a few to a hundred millitorr. Immediately after applying a voltage to the cathode, electrons will be emitted from the negatively charged electrode and hit neutral gas atoms on their way. Upon their collision one electron is detached from the outer shell of neutral gas atoms rendering them positively charged. These positively charged ions impinge on the surface of the target material and the sputtered atoms form a thin film on the substrate placed on the anode subsequently.

2.4.2 DC magnetron sputtering

The considerable drawbacks with diode sputtering such as low sputtering rate, cathode oxidization[11] and low probability of impacting secondary electrons with sputtering gas because of electrons dispersion inside the chamber, has led to the development of a new sputtering configuration called magnetron sputtering. Thanks to the magnets mounted behind the cathode, electrons are trapped in the magnetic
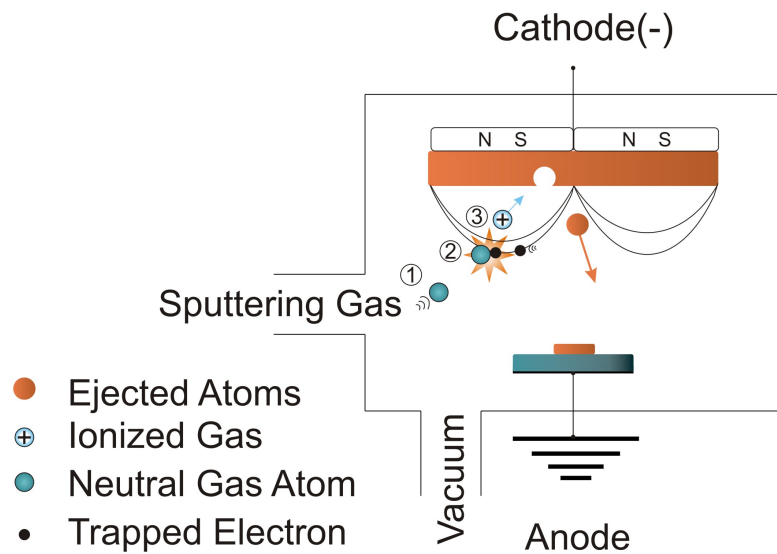
Figure 2.7: A schematic illustration of magnetron sputtering,(1) Argon gas is pumped into the chamber ever existing electrons inside the chamber ionize Argon gas atom (2) Argon gas ions hit the target and sputter it(3)

field preventing them from bombarding of the substrate, which is an important disadvantage in the former sputtering technique. In addition, the presence of electrons in the proximity of the target increases the chance of ionizing gas atoms leading to a higher sputtering rate. The configuration of this system has been presented in (Figure 2.7). Depending on the configuration of the magnets there are different types of magnetron sputtering such as cylindrical post magnetron, magnetron gun and planar magnetron[11]. Figure 2.7 shows the magnetron sputtering process schematically.

2.4.3 Reactive sputtering and related issues

Compound thin film coatings could be sputtered either by using a compound target directly or by introducing a reactive gas along with the working gas into the chamber. It is reported that fabricating ductile metal targets with acceptable purity is much more convenient than fabricating brittle compound target with the same purity; hence the purity of the sputtered compound thin films are much higher by employing highly pure reactive gases. However, controlling the stoichiometry and microstructure of the resultant thin film is very challenging due to the instability of the plasma. This instability in plasma stems from a hysteresis behavior revealed when certain parameters such as nitrogen partial pressure, plasma power and current are modified. This phenomenon is commonly explained in literature by the sputtering yield difference between compound and metal. In (Figure 2.8) this effect can be observed where the processing curves for plasma intensity as a function of DC power in the TiN reactive sputtering has been plotted and compared with the non reactive Ti sputtering with only pure argon. The argon and nitrogen gas flow rates are kept constant at 40 sccm and 4 sccm respectively. As can be observed there is no significant increase in Ti signal until point 1. This indicates that almost all nitrogen in the
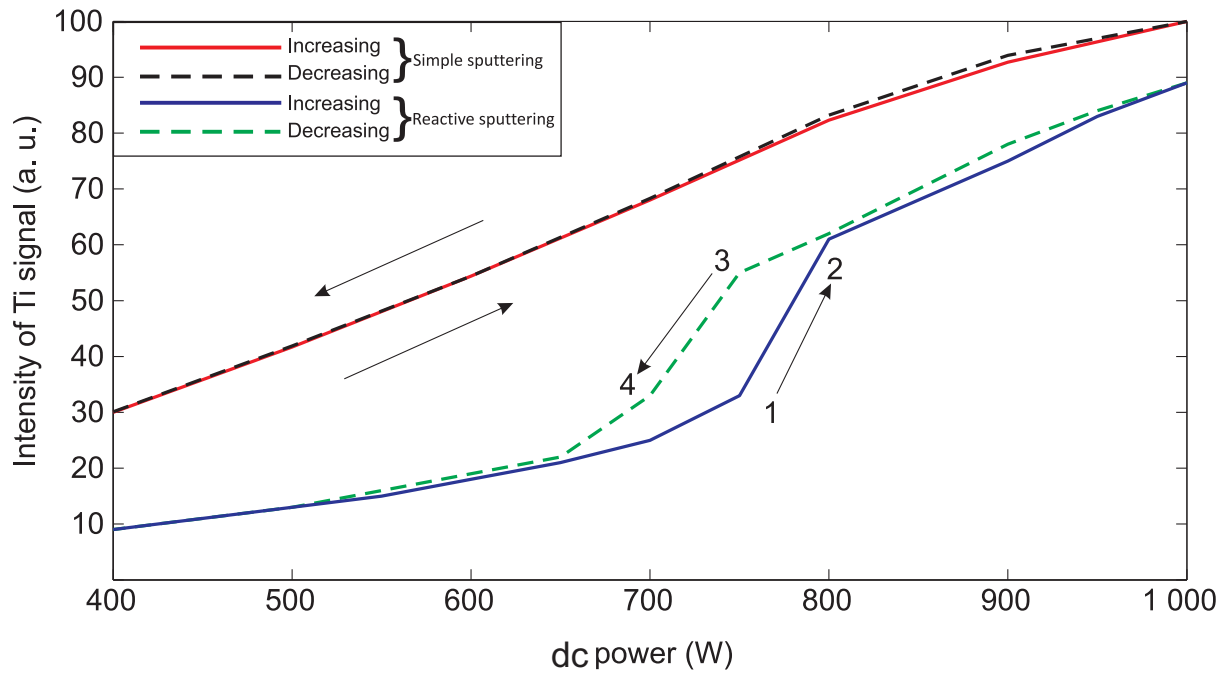
Figure 2.8: Plasma intensity of Ti signal versus plasma dc power

chamber is consumed to form a TiN layer on the target surface. The target is said to become poisoned at this point. Since the sputtering yield of TiN is less than pure titanium the deposition rate is in its minimum state. As the plasma, power increases the Ti signal increases abruptly to point 2. Here the target operates in metallic mode where the built up TiN layer is eroded by higher power plasma leading to sputter titanium nitride on the substrate. As the power decreases to point 3 the TiN layer gradually is formed on the target until it reaches to point 4 where the target returns to poisoned mode.

The same hysteresis appears while the nitrogen flow rate increases stepwise and other parameters kept constant (Figure 2.9) . As the nitrogen flow rate increases the nitrogen partial pressure initially remains relatively constant until point 1 after which follows a sharp increase of the nitrogen partial pressure to point 2. This shows that initially all nitrogen is consumed to form TiN and then the unused nitrogen builds up the nitrogen partial pressure. It should be noted that in contrast the former case, the first steep transition is between the poisoned mode and the metallic mode. In the reverse path the the target is being eroded and the nitrogen flow rate decreases simultaneously.This results in the emergence of the metallic mode which is accompanied with a dramatic decrease in the nitrogen partial pressure to the point 4. The sudden transition between point 1 and 2 in the pressure figure correlates with a change in film crystal structure from hexagonal closed pack (h.c.p) to face-centered cubic (f.c.c)[9].

The hysteresis behavior was the main obstacle in our way when aiming to fabricate stoichiometric TiN with an acceptable level of reproducibility. In order to address this problem we first develop a method which minimizes the hysteresis effect and then find an optimum point in the hysteresis where we can achieve stoichiometric TiN.

Bergs model [12] has been suggested to describe the sputtering process as predictable as possible. In this model although all of the involved factors are not considered, it simplifies the process to a large extent which leads to more controllability. Based on this model the shape and the surface of the hysteresis is mainly affected by two groups of factors; those related to materials and those related to process-
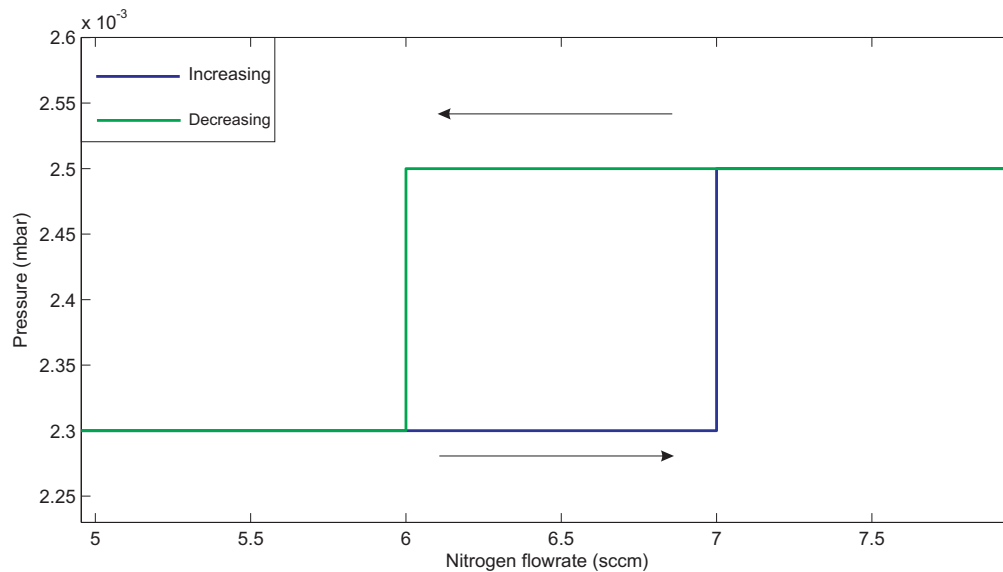
Figure 2.9: Pressure of the chamber versus Nitrogen flow rate

ing.Since we are not free to change the materials we put our emphasis on the latter group. For instance, from the former group it is reported that the reactivity between the gas and the target plays an important role in the hysteresis effect [13]. Sputtering yield is among the parameters that highly affects the hysteresis shape. When the difference between the sputtering yield of the compound and metal is small the hysteresis becomes negligible [14].The pumping speed is a parameter which belongs to the latter group.The higher the pumping speed the smaller the hysteresis [15].

2.4.4 x-Ray photoelectron spectroscopy (XPS)

X-ray photoelectron spectroscopy (XPS) or electron spectroscopy of chemical analysis (ESCA) is one of the most widely used surface analysis methods due to its relative simplicity in use and data interpretation. In this method electrons from a core level of the studied material are ejected as a result of X-ray irradiation, followed by energy analysis of the emitted electrons by an electron spectrometer (Figure 2.10). As a result, a graph of intensity versus electron binding energy is obtained. Although the kinetic energy of the ejected electron can be measured by spectroscopy, this is not an intrinsic property of the specimen considering the electron energy dependency on the photon energy of the irradiating X-ray. The binding energy (EB) of the electron is the energy by which the electron can be identified. The formula that considers all parameters involved in XPS is: EB=hv-EK-W where EB is the binding energy of the electron, hv is the photon energy ,EK is the kinetic energy of the electron and W is the spectrometer work function. All these parameters are measured automatically by the XPS tool and EB is extracted. Consequently, based on the resultant graph the chemical composition of a compound and the existence of impurities can be revealed.

As mentioned previously XPS is a surface analysis method allowing analysis up to 10 nm in depth. Hence,many XPS tools are equipped with an argon sputtering gun which can sputter a thin layer from the surface prior to the analysis. However by this method the sample could be damaged and modified. M. Delfino et al. [16] have developed a technique that circumvents this problem by employing an XPS
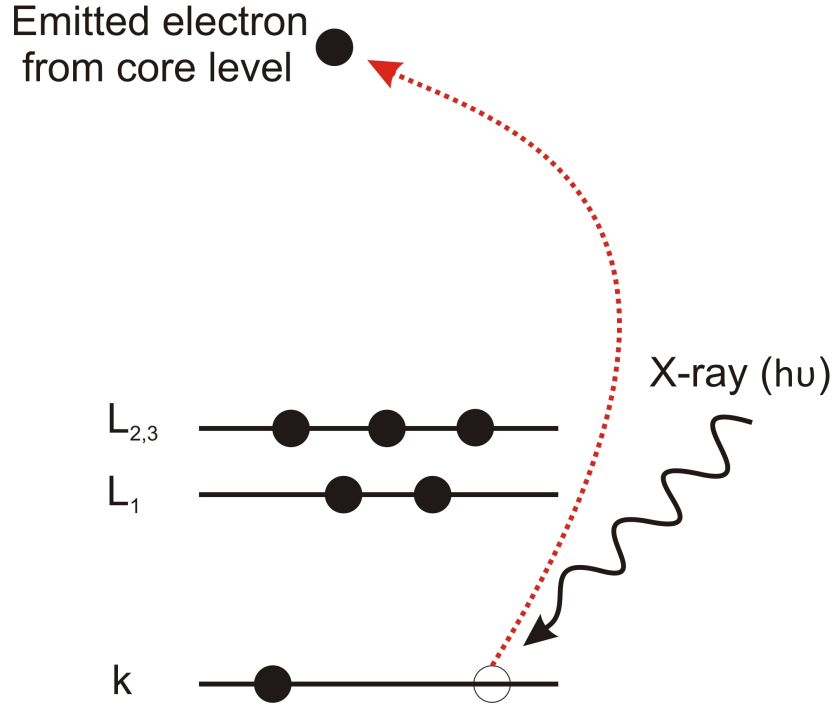
Figure 2.10: A schematic illustration of X-Ray photoelectron spectroscopy principle

analytical module to the central handler of the sputtering tool for analyzing reactively sputtered TiN where the XPS analysis can be performed in-situ.

We have adopted XPS to identify the stoichiometry of the sputtered TiN films and also the chemical bonding state of TiN.

2.4.5 Four-point-probe resistivity measurement

The resistivity of the produced TiN thin film under different sputtering condition has been continuously measured in this work. The principle of this technique is schematically presented in (Figure 14). Current is supplied through the outer probes and the voltage drop across the thin film is measured via the inner probes simultaneously. The resistivity (ρ) is an intrinsic characteristic of the material while the sheet resistance is the resistance of a thin sheet of material. The tool consists of a probe head (Figure 2.11) and a mechanical instrument which provides sufficient force to connect it to the surface of the studied sample. The tip radius of the used probe head was 200 μm and the spacing between the probes were 1 mm. For equal spacing probe heads, very thin (thickness t$\ll$s)and very wide (lateral dimension (d$\gg$s)sample the resistivity is given by:

$$\rho = \frac{\pi}{ln(2)} t \left(\frac{V}{I} \right) = 4.5324t \left(\frac{V}{I} \right)$$

where I is the applied current, V is the voltage measured by the voltmeter and t is the thickness of the film. Based on the studied sample size (10x10 mm) the above formula must be corrected for laterally finite geometries with an appropriate correction factor. These correction factors have been already calculated by F.M Smith et al.[17]. Based on the provided table and the ratio between the width and the probe
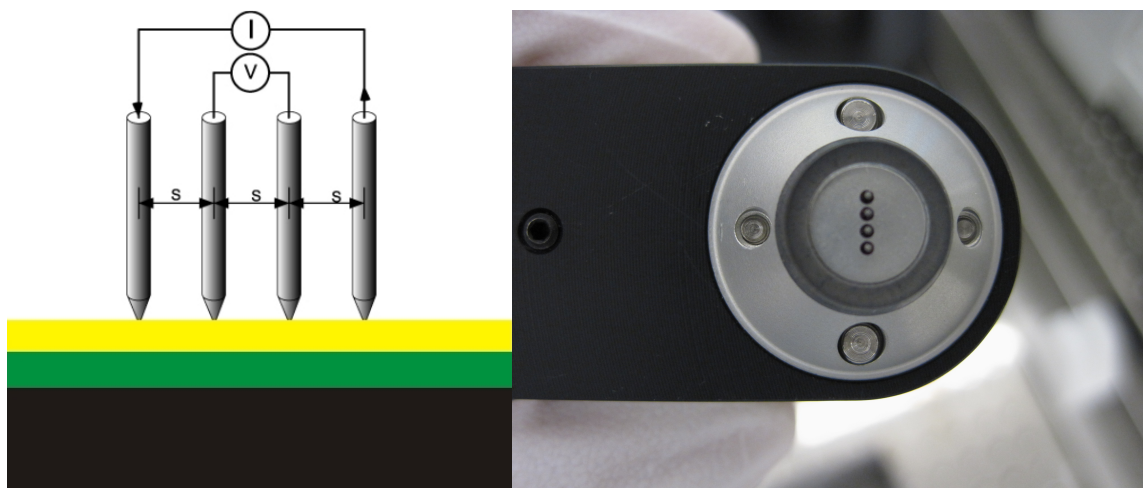
Figure 2.11: Schematic illustration of four-point probe resistivity measurement (left),A typical probe
head(right)

spacing (d/s) a coefficient of 0.93 is multiplied by the above formula. In order to obtain an accurate
value for the resistivity the thickness of the film were measured by surface profilometry technique and
subsequently multiplied by the sheet resistance obtained by four-point probe measurement tool. The
measurement procedure will be thoroughly explained in the following chapter.

3 Experiment

In essence our experimental works is divided into two sections; TiN fabrication using two different dc magnetron reactive sputtering tools followed by characterization and assessment of the produced TiN film as the underlayer. The sputtering tools used for the former part were Nordiko 2000 and FHR MS 150x4-L in the chronological order. For the latter part, resistivity measurements accompanied with thickness measurement using four-point probe tool and surface profiler (Tencor P15), scanning electron microscopy (SEM) after annealing and growth of VACNFs, and X-ray photoelectron spectroscopy (XPS) are available. In the followings, we give a technical description of the used tools and then the experimental conditions will be thoroughly explained.

3.1 Hole-mask colloidal lithography

In order to deposit the nickel catalyst seeds on the TiN substrates for annealing tests and VACNFs growth studies, we adopted a convenient, cost efficient and high throughput method called hole-mask colloidal lithography. A step by step schematic illustration of the method is presented in (Figure 3.1). As Figure 3.1 shows the process starts when Polymethyl methacrylate (PMMA) acting as a sacrificial layer is spin coated on top of the TiN layer (Figure 3.1.c). This is followed by 5 seconds low power oxygen etching in order to increase its hydrophilicity. Then a negatively charged electrolyte layer is pipetted on top called Polydiallyldimethylammonium (PDDA) (Figure 3.1.d). Subsequently, the positively charged nanospheres (sulfate latex) with 80 nm diameter are pipetted and attached to PDDA layer through the electrostatic force between them (Figure 3.1e). Subsequently a 10 nm of gold film is deposited on top of the stack in an electron beam evaporation tool (AVAC) (Figure 3.1.f). This step is followed by detaching the nanospheres from the surface by a special tape which results in a hole-mask pattern (Figure 3.1.h). The distances between these holes are determined by the electrostatic forces between the nanospheres. The PMMA layer underneath the holes in the gold is etched in an oxygen plasma (Figure 3.1.i). Finally Ni catalyst is deposited (Figure 15.j) followed by a lift off process. Consequently the colloidal pattern is transferred to the TiN substrate (Figure 3.1.k). In the SEM micrographs leftmost one shows the gold hole-mask and the rightmost one shows the substrate after Ni deposition (Figure 3.2).

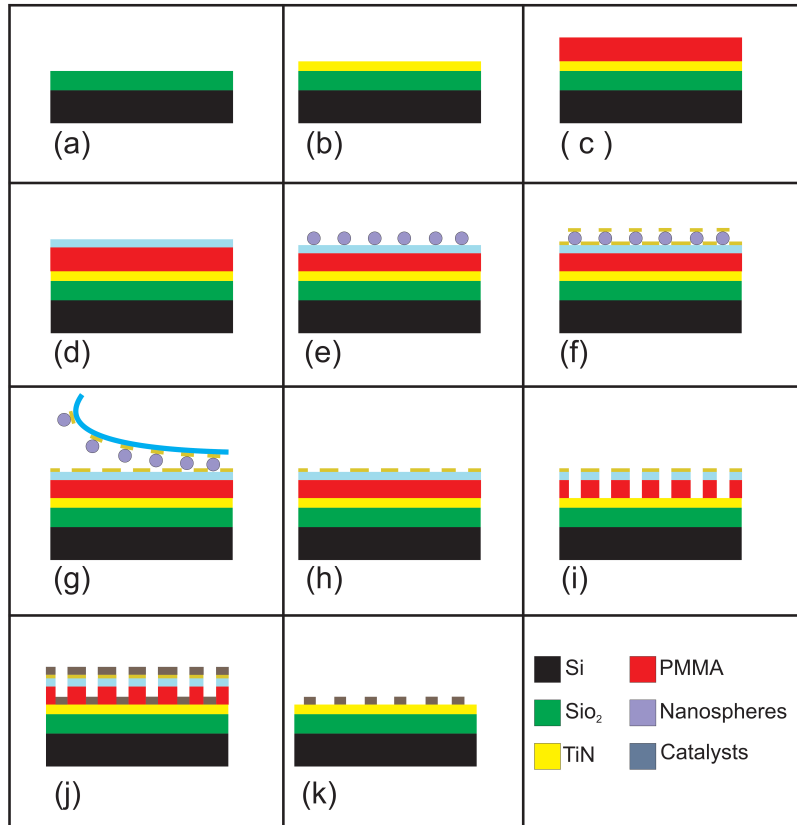Figure 3.1: A schematic illustration of hole-mask colloidal lithography
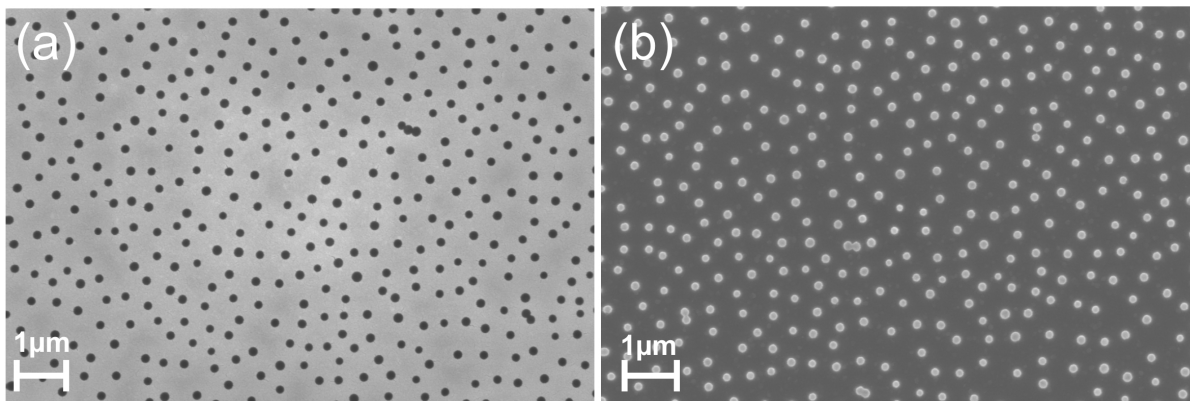

Figure 3.2: SEM micrographs of (a) gold hole-mask (b) Ni seeds on top of TiN after lift-off

3.2 TiN reactive sputtering

Nordiko 2500

In Nordiko the samples are placed into a stainless steel chamber, which has a 50 mm wide viewing window to see the plasma while it is ignited. The relatively large volume of the chamber needs at

least 8 hours to be well evacuated before initiation the sputtering process. Three separate electrodes are connected to a DC power supply. If RF sputtering required it is also possible to connect one of the electrodes to an RF supply. The machine has four individual targets and corresponding water-cooled substrate tables.

The distance between substrate and target is adjustable but normally it is fixed to the maximum distance (45mm). The position of the tables is controllable via a computer, which is connected to the base plate driver motor. The chamber is connected to a rotary vacuum pump and a mechanical pump. The pressure of the chamber is controlled by Balzers TPG 300 controller based on the received data from the Pirani and Penning gauges mounted on the system. The pressure can be ranged from atmosphere pressure to 10^{10} mbar. Three different gases (Ar, N_2, and O_2) are connected to the chamber and their flow rates are regulated by mass flow controllers. The pressure of the chamber after introducing the desired gases can be regulated by an automatic throttle valve.

3.2.1 Evaluating the diffusion barrier performance of TiN

In order to investigate the effect of temperature on the diffusion barrier performance of the TiN film, the samples were heated to the three different final temperatures; 500°C, 600°C and 700°C with the same ramp rate of 100°C/min.

3.2.2 Effect of Nitrogen partial pressure on TiN film

Referring to Sundgren et al. [18] the effect of partial pressure of nitrogen on the sputtered TiN film was investigated. A 3 inch silicon wafer with 400nm thermally silicon dioxide layer on top, were spin coated with a common primer Hexamethyldisilazane (HDMS) followed by negative photo resist S1813 in order to protect it from damage during dicing. The 10×10 mm^2 diced chips were cleaned using 1165 remover and isopropyl alcohol (IPA) solution ultrasonically. In order to measure the thickness of the sputtered film by surface profiler TENCOR P.15 the chips were patterned by photolithography (Figure 3.3). For consistency in the thickness of the TiN the deposition rate of TiN and Ti were calculated. Two chips were always placed onto the substrate turning holder opposing together in 90°with respect to each other. Prior to sputtering the flow rates of argon and nitrogen were set to 24 sccm and 1 sccm respectively. After introducing gases in to the chamber the plasma was ignited and the processing pressure was set to 2.3 mtorr. The chips were pre sputtered for 60 minutes in order to clean the chamber and to obtain plasma stability. The plasma current was kept constant (current regulated) at 0.8 A during the sputtering. Both Ti and TiN chip were sputtered for 60, 90,120 s.

Keeping the deposition rate as a reference we started to run the main experiment where the nitrogen gas flow rate was modified as it is shown in (Table 3.1). For all of the trials the chamber was evacuated for 12 hours reaching to acceptable base pressure (Table 3.1). Each time four chips were loaded in the chamber; one for evaluating the quality of the grown VACNFs in the PECVD chamber, one chip for evaluating the diffusion performance of the TiN film after annealing, one for resistivity measurement and one patterned chip for thickness measurement (Figure 3.3). After pre-sputtering the samples were sputtered with different nitrogen partial pressure. The resistivities of the produced films were measured using the four point probe method. The diffusion barrier performance of the samples was evaluated after annealing by SEM. The samples were heated up for 600°C, 650°C and 700°C final temperatures (100°C per minute).The growth step was performed while theC_2H_2 / NH_3 mass flow ratio was kept constant at

0.25. The VANCFs were analyzed by scanning electron microscopy (SEM).
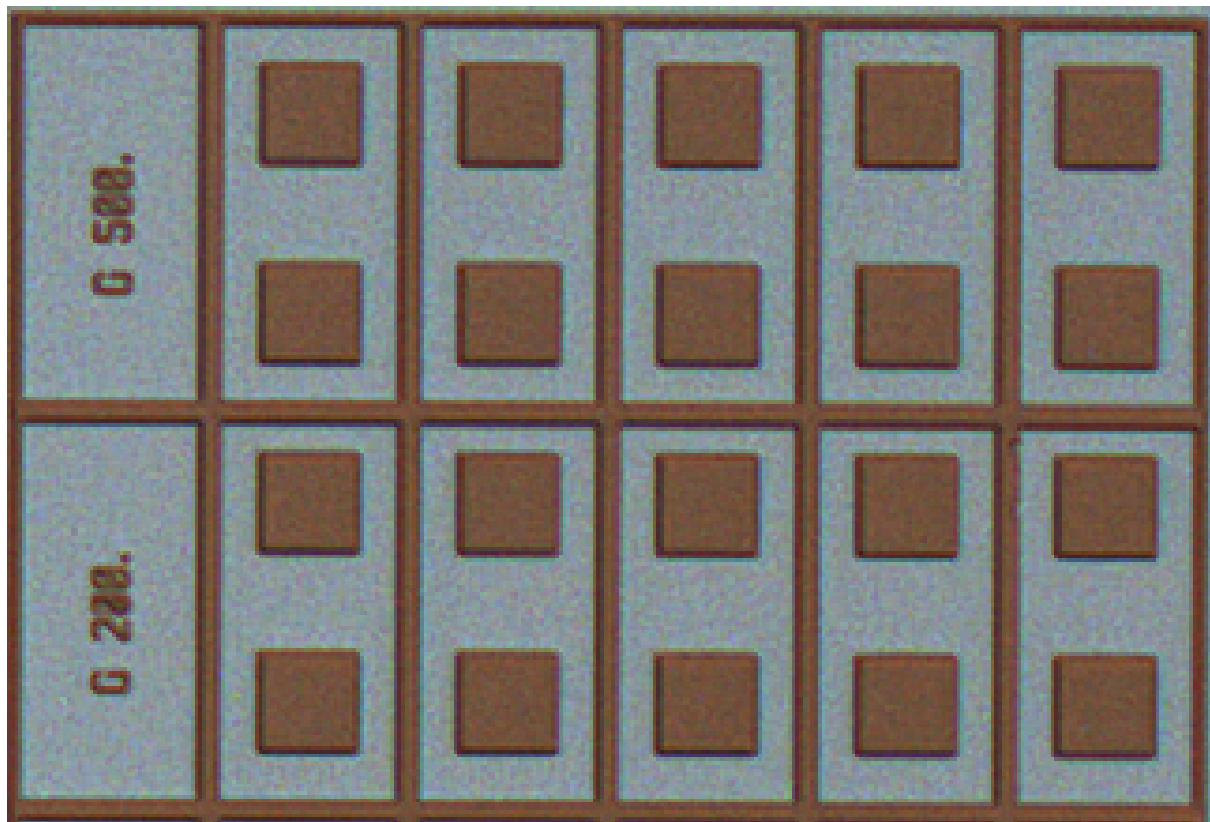

Figure 3.3: Thickness measurement chip patterned by photolithography for use in surface profiler

Table 3.1: Sputtering parameters for the partial pressure experiment

Sample No.	Chips ID	Total Pressure	Nitrogen Mole percent	Nitrogen partial pressure	Nitrogen Flow Rate	Argon Flow rate	Base pressure
1	Chip A-r Chip B-a Chip C-g	2.5 mtorr	0%	0.0 mtorr	0 sccm	24 sccm	2.8×10^{-6} mbarr
2	Chip A-r Chip B-a Chip C-g	2.5 mtorr	4%	0.1 mtorr	1 sccm	24 sccm	2.8×10^{-6} mbarr
3	Chip A-r Chip B-a Chip C-g	2.5 mtorr	10%	0.25 mtorr	2 sccm	18 sccm	3.6×10^{-6} mbarr
4	Chip A-r Chip B-a Chip C-g	2.5 mtorr	20%	0.50 mtorr	4.5 sccm	18 sccm	3.6×10^{-6} mbarr
5	Chip A-r Chip B-a Chip C-g	2.5 mtorr	25%	0.625 mtorr	6 sccm	18 sccm	3.9×10^{-6} mbarr
6	Chip A-r Chip B-a Chip C-g	2.5 mtorr	50%	1.25 mtorr	12 sccm	12 sccm	3.9×10^{-6} mbarr
7	Chip A-r Chip B-a Chip C-g	2.5 mtorr	66%	1.66 mtorr	16 sccm	8 sccm	3.9×10^{-6} mbarr
8	Chip A-r Chip B-a Chip C-g	2.5 mtorr	100%	2.5 mtorr	24 sccm	0 sccm	3.9×10^{-6} mbarr

[1] R,a,g stand for resistivity ,annealing and growth respectively.

3.2.3 Target- Substrate spacing

The effect of the distance between the substrate and the Ti target was investigated. Four 10*10 mm2 silicon chips with 400 nm sio_2 on top were cleaned ultrasonically in acetone and rinsed and nitrogen dried prior to loading into the chamber. The pressure of the chamber before introducing the gases was 1.6×10^-6 mbar. The distance between target and substrate was set to its maximum state which is 45 mm. After introducing argon and nitrogen gases at 18 and 2 sccm respectively into the chamber, the process pressure was set to 2.5 mbar. The plasma current was set to 0.8 A. Prior to opening the shutter the target was pre sputtered for 60 seconds. Knowing the deposition rate for this target-substrate configuration the samples sputtered for 6 minutes resulted in approximately 300 nm TiN which allows us to observe the film in SEM more conveniently. The experiment was repeated with minimum distance while the other

parameters remained unchanged. The microstructure of the TiN film was studied using SEM.

FHR MS 150×4-L

FHR is a magnetron sputtering system equipped with two separate chambers. The first is an aluminum made handling chamber in which the substrate carrier is placed inside and subsequently transferred to the processing chamber via a fork like arm after being evacuated to vacuum pressure. The second is a stainless steel process chamber in which three DC and one RF sputter sources are installed. The handling chamber is evacuated by either a turbomolecular pump or a backing pump while the pressure is measured via a Pirani and Penning vacuum gauge installed at the bottom section of the chamber. This configuration makes sure that the process chamber is always in vacuum pressure while in the former system (Nordiko) it takes at least 8 hours for the process chamber to be evacuated. In addition to these gauges the process chamber has a Baraton gauge functioning as the process control sensor. The working and reactive gases (O_2, N_2, Ar) are entered in the process chamber through a gas control module with three VCR-type gas lines consisting of a manual valve, a filter, a mass flow controller (MFC) and a pneumatic cut-off valve. There are six stations on which the substrate carriers can be positioned and turned depending on the desired sources to be sputtered. One of these stations can be heated up to 600°C by a resistive heater and another can be water cooled. There is however a large tolerance between the real temperature of the substrate and this value because of high thermal resistance at the heater-carrier interface and also between the carrier and the substrate. The temperature of the substrate can be monitored and controlled according to the data sent from a pyrometer.

As mentioned above it is very challenging to reactively sputter stoichiometric compound thin films due to the instability of the discharge. FHR benefits from an optical emission spectroscopy (OES) tool that is able to visualize plasma intensity. OES functions by detecting the radiation emitted from plasma by an optical fiber and visualizing it based on its wavelength patterns. It should be noted that in contrast to other plasma diagnostic methods such as electrical probes, OES is a passive technique meaning that it does not interfere with the plasma [19].The optical emission of plasmas is widely used for stabilization of the process by taking metal emission signals as an input for regulating the flow rate of the reactive gas considering the fact that the emission intensity of any line of the metal target is proportional to the metal fraction of it. In the FHR there is a UPC03 controller which is connected to the spectrometer and which controls the reactive gas flow rate. Unfortunately due to malfunction of the controller we were forced to control the process manually.

In addition to these beneficial features, there is a user-friendly visualization software installed on the machine by which all of the parameters involved with the sputtering process can be monitored and recorded (within 1 second intervals). In (Figure 3.4) an overview of the process screen is shown.

3.2.4 Hysteresis effect experiment

The hysteresis in reactive sputtering is investigated by modification of plasma power, current and reactive gas flow rate. The color of the film is always taken into account as a simple and quick reference to approximately estimate the deviation from stoichiometry. Ph. Roquiny et al. [8] show that the color of the titanium nitride film changes from metallic grey to dark brownish and also goldish in the middle for the stoichiometric TiN as the nitrogen content of the film increases. The hysteresis experiments are dived into three categories as follows:

- Hysteresis effect as function of nitrogen flow rate:As a first series of experiments from this cat-
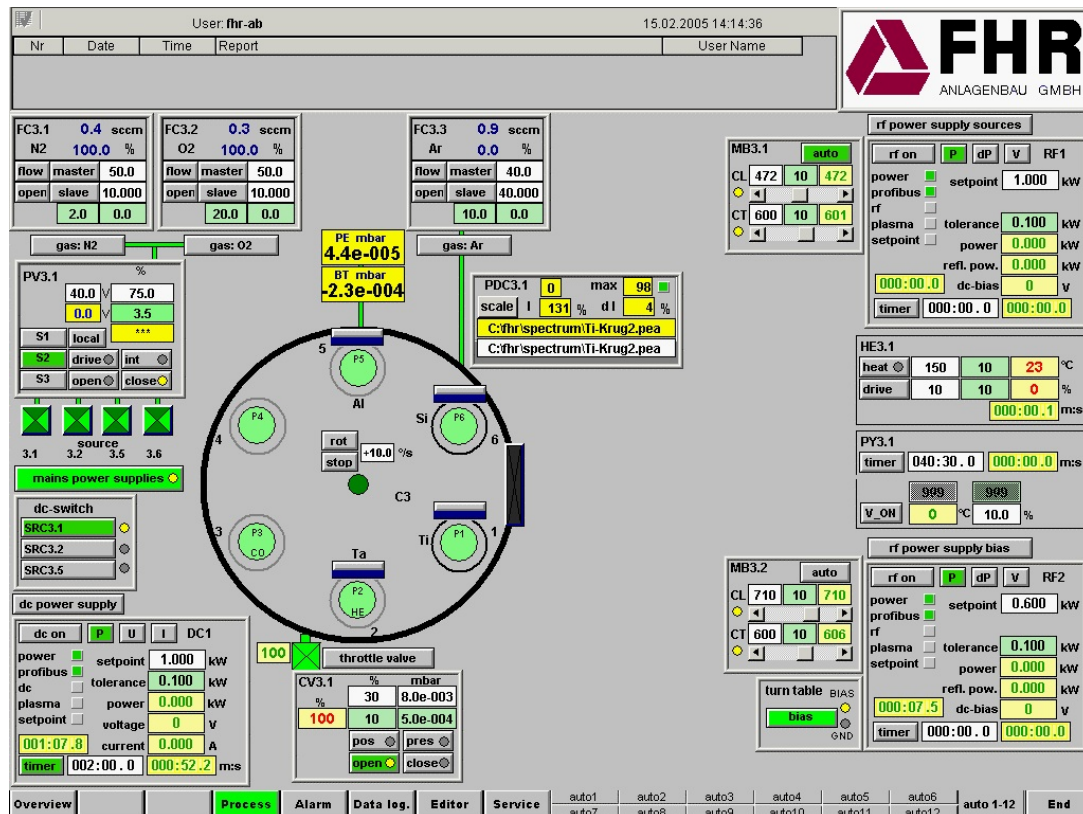
Figure 3.4: An overview of the process control UI of the FHR sputtering system

egory the effect of nitrogen flow rate was investigated. In order to run this a dummy chip was loaded into the chamber. The plasma power was fixed at 1 kW and the chamber valve was in fully open state. The substrate RF bias power was kept at 600 W. Initially the argon and nitrogen flow rates were regulated at 40 sccm and 3 sccm respectively. After 1 minute the argon pre-sputtering the nitrogen flow rate was increased stepwise. We stayed at each flow rate until the plasma intensity become relatively stable without huge fluctuation. We proceeded up to 10 sccm and then reduced the N2 flow to 3 sccm. Plasma intensity, chamber pressure and voltage were recorded in all the trials.

• Hysteresis effect as function of plasma power:The plasma power was increased from 300 W to 900 W while all the other parameters were kept constant. As soon as the plasma intensity reached to stability the plasma power was increased and decreased step wise.

• Hysteresis effect as function of plasma current:The plasma current was increased from 1.75 A to 2.1 A and was then returned from 2.1 A to 1.75 A while the other parameters remained unchanged.

The experiments parameters are summarized in (Table3.2).

3.2.5 Minimizing the hysteresis area

Based on the theoretical modelling by Berg wt al. it has been concluded that an increased pumping speed will significantly reduce the hysteresis area [12]. Unfortunately due to the limitation on modifying the

Table 3.2: Hysteresis experiment sputtering parameters

Trials No.	Argon flow rate(sccm)	Nitrogen flow rate(sccm)	Base pressure (mbar)	Plasma power (W)	Plasma current (A)	RF bias (W)	Throttle valve position
1	40	3 $\Longleftrightarrow$ 8	6.10×10^{-7}	1000	2.7	600	Fully open
2	40	4	3.30×10^{-7}	1000 $\Longleftrightarrow$ 400	Varied in accordance with power	600	Closed
3	40	4	5.0×10^{-7}	Varied in accordance with current	1.75 $\Longleftrightarrow$ 2.1	600	Closed

pumping speed in FHR and in view of the fact the speed required for eliminating the hysteresis is too high to reach [20], we developed a new approach in order to minimize the hysteresis. In this experiment the argon gas flow rate was increased two fold (80 sccm) and then nitrogen gas flow rate was set at 4 sccm, while the throttle valve was kept thoroughly opened. The experiment was carried out in current regulated condition meaning that the plasma current ranged from 1.75 A to 2.1 A and vice versa. The plasma intensity was recorded while the process was in progress.

3.2.6 Current regulated sputtering experiments with and without substrate Rf bias

Pursuing the sputtering of TiN, we modified the DC magnetron current and monitored the plasma intensity response from the optical spectrometer. We found out that this method offered more stability and reproducibility in comparison to the former method of changing partial pressure of nitrogen. In order to equalize the thickness of the TiN films in all of the trials, we kept the sputtering time constant at 180 seconds and the corresponding deposition rates were calculated consequently.

Four 10×10 mm2 plain chips with thermally grown 400-nm-thick SiO_2 and one photolithographically patterned chip for thickness measurement by surface profilometry were loaded into the chamber. Two of the chips were considered for resistivity measurement and the two others were considered for annealing and VANCF growth assessment. Station 2, on which a dummy wafer is placed, rotates to be positioned under the target. The 92 sccm argon gas entered to the chamber and plasma was ignited with initial plasma current of 1.6 A. The target was pre sputtered for 60 seconds by only pure argon gas. Then the nitrogen gas was let in to the chamber at a constant 3 sccm and the final plasma current was set simultaneously. The plasma intensity dropped abruptly and continued slightly decreasing until it became relatively stable. At this point the shutter was opened and the dummy chip on station 2 was sputtered for 60 seconds. These steps prior to the main sputtering process on station 1 were carried out in order to stabilize the plasma as much as possible. The instability in the plasma as a result of the shutter position will be discussed later. The sheet resistance of the sputtered TiN films was measured in a four-point-probe apparatus within 2 minutes after the chips were taken into atmosphere in order to minimize the adverse effect of oxidization. The exact thickness of the resultant TiN films were measured by a surface profilometry system (Tencor P15) and multiplied by the corresponding sheet resistance to find the resistivity. The annealing of the nickel catalysts and VACNFs synthesis were carried out in an AIXTRON Black Magic PECVD reactor. In the annealing step the samples were exposed to 650°C

within about 6 minutes (100°C per minute) in NH_3 ambient.

In order to investigate the effect of RF bias on the substrate the experiment was repeated under the same condition while the substrate was grounded.

4 Results and Discussion

4.1 Annealing at different final temperature

Figure 4.1 shows the diffusion barrier performance of unoptimized sputtered TiN and the corresponding VACNFs growth at different final annealing temperature. This indicates that although we have deposited 50 nm thick Ni at 700°C almost all the Ni seeds have disappeared resulting in very poor VANCNFs growth. This calls for an optimization of the sputtering condition to yield denser and enhanced quality TiN film which is the main focus of our work as explained in the following.
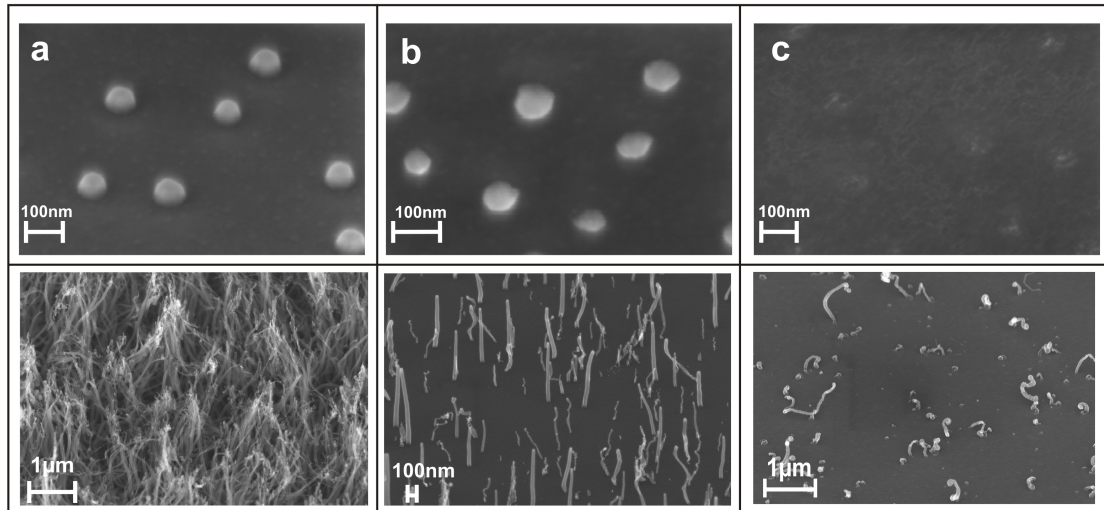
Figure 4.1: Annealing and corresponding VACNFs growth at a 500°C , b 600°C and c 700°C final temperature with 100°C/min ramp rate

4.2 Target-substrate spacing

Figure 4.2 shows two SEM micrographs of the TiN films; the right one was sputtered at maximum target-substrate spacing (a) and the left one was sputtered at minimum target-substrate spacing (b). As can be observed there is no significant difference in the microstructure of the film as revealed by SEM.

However there is a huge difference in the deposition rate. Kumar et al. claim that as the distance between target and substrate becomes smaller a higher number of sputtered neutrals are available [21].
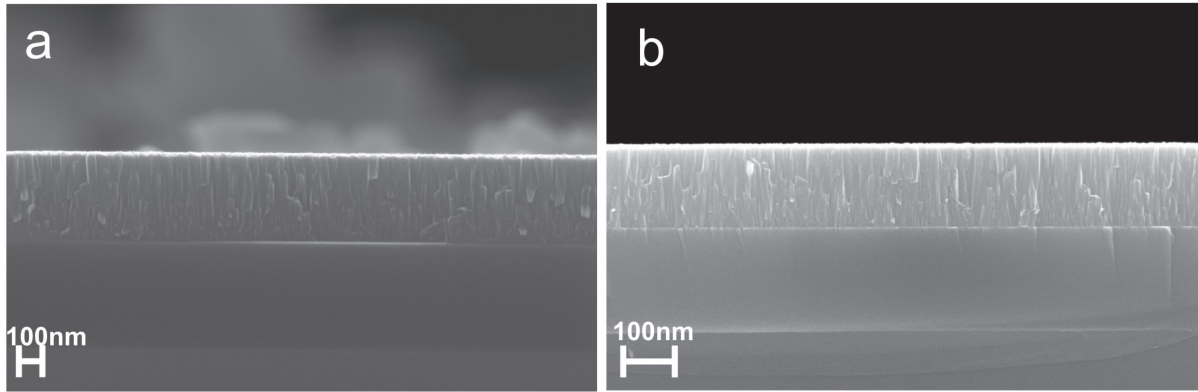
Figure 4.2: SEM micrographs of sputterd TiN at (a) maximum distance and (b) minimum distance

Table 4.1: Add caption

Target-substrate distance	Maximum Target-substrate distance	Minimum Target-substrate distance
Resistivity	$175\mu\Omega$ .cm	$137\mu\Omega$.cm
Deposition rate	12 nm/minute	127 nm/minute
Microstructure	Refer to SEM micrograph	Refer to SEM micrograph

4.3 Nitrogen partial pressure

Pure titanium in argon ambient and TiN in N_2 and Ar mixture were sputtered in three courses of time in order to find the deposition rate. As Figure 4.3 shows the deposition rate of Ti is higher than the one for TiN.
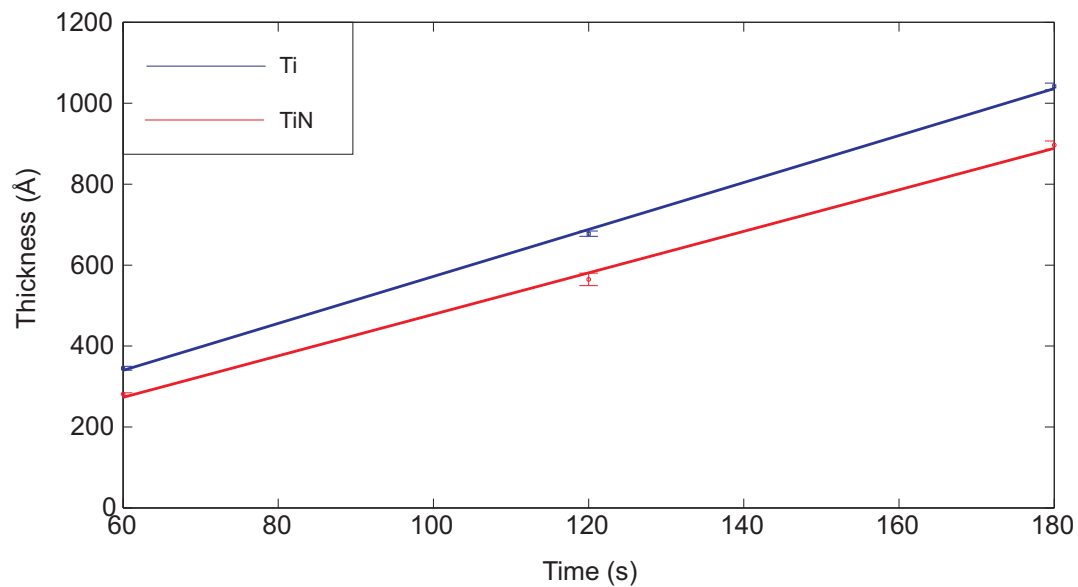
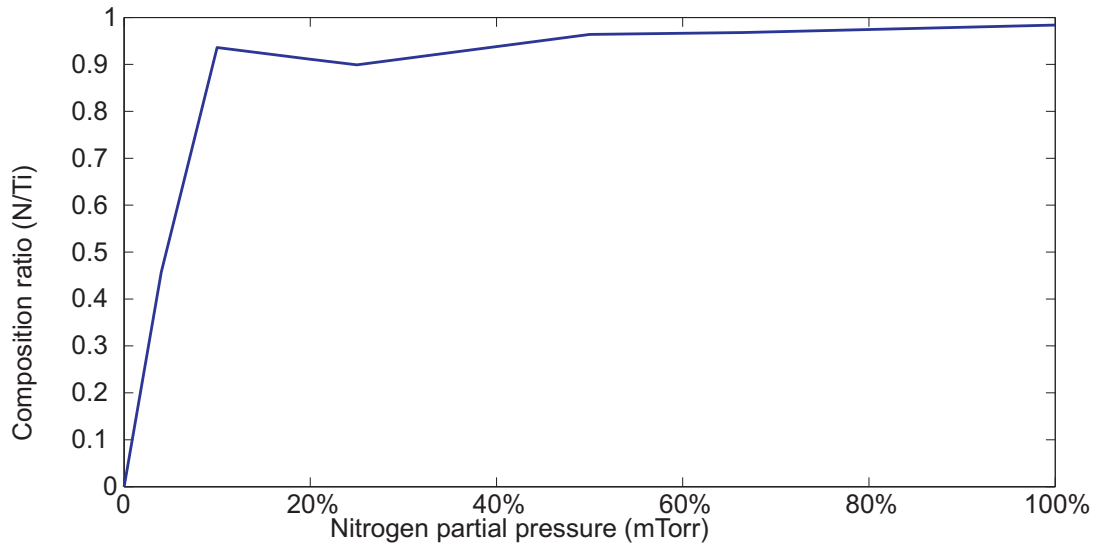Figure 4.3: Deposition rate of Ti and TiN

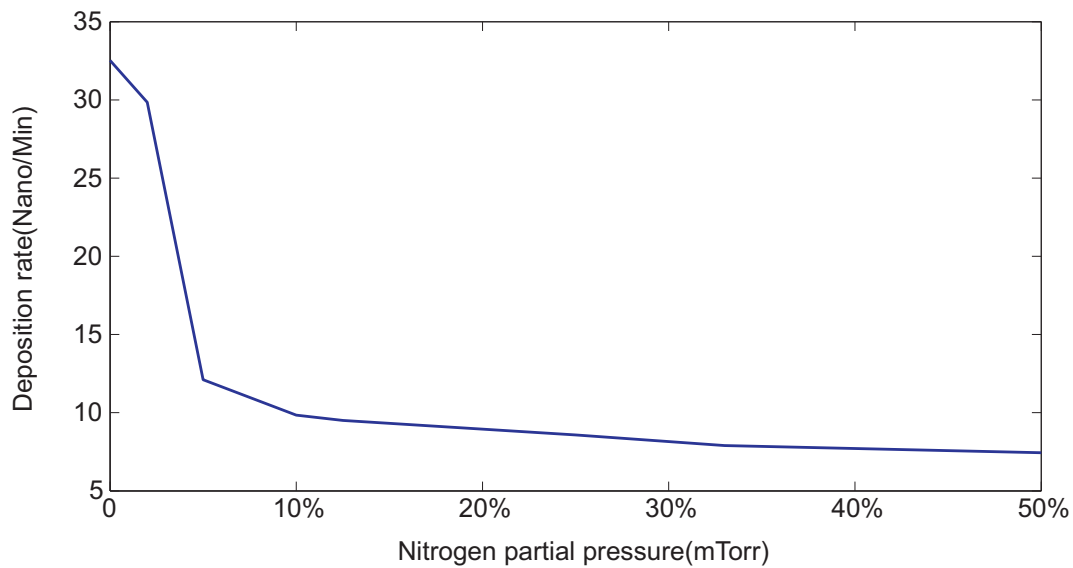Figure 4.4: TiN composition ratio as a function of nitrogen partial pressure

Figure 4.5: Deposition rate of TiN as a function of nitrogen partial pressure

The reason for this is formation of a compound with lower sputtering [6] on the surface of the target (pure titanium). The sputtering kinetics of this nitride layer on the target has been observed and reported by Sundgren et al. After this reduction in deposition rate the target is said to be poisoned. This layer has a role in the growth of the sputtered film. In addition Figure 4.5 shows at a nitrogen partial pressure of 25% the deposition rate becomes relatively steady indicating that the target is fully poisoned. Sundgren et al. reports that at this point further increment in nitrogen partial pressure does not affect the composition ratio of TiN. This is in agreement with our observation as shown in (Figure 4.4). As discussed in paper A, the diffusion barrier performance and VACNF growth improves by increasing nitrogen content of the

film as a result of nitrogen partial pressure increase. Although, based on our XPS data, the film has become stoichiometric at 10% nitrogen partial pressure the resistivity is one order of magnitude higher than what is reported for stoichiometric TiN. This shows that other parameters such as tensile stress generated in the grain boundaries [18] as a result of low energy at substrate during sputtering might be involved in the resistivity of TiN films.

4.4 Hysteresis effect

In (Figure 4.6) the appeared hysteresis effect as a function of dc plasma power, nitrogen gas flow rate (Figure 4.7) ,dc plasma current (Figure 4.8), is shown. Based on these experiments we came to the conclusion that plasma intensity shows more stability when it is controlled by plasma current. So we proceeded to sputter TiN films at different magnetron current inside the hysteresis area.
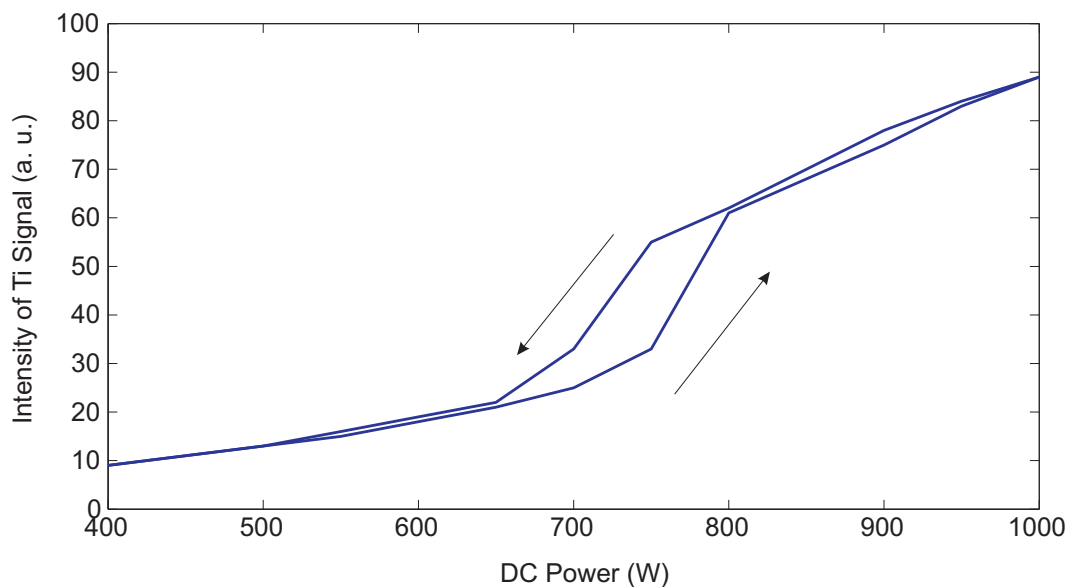

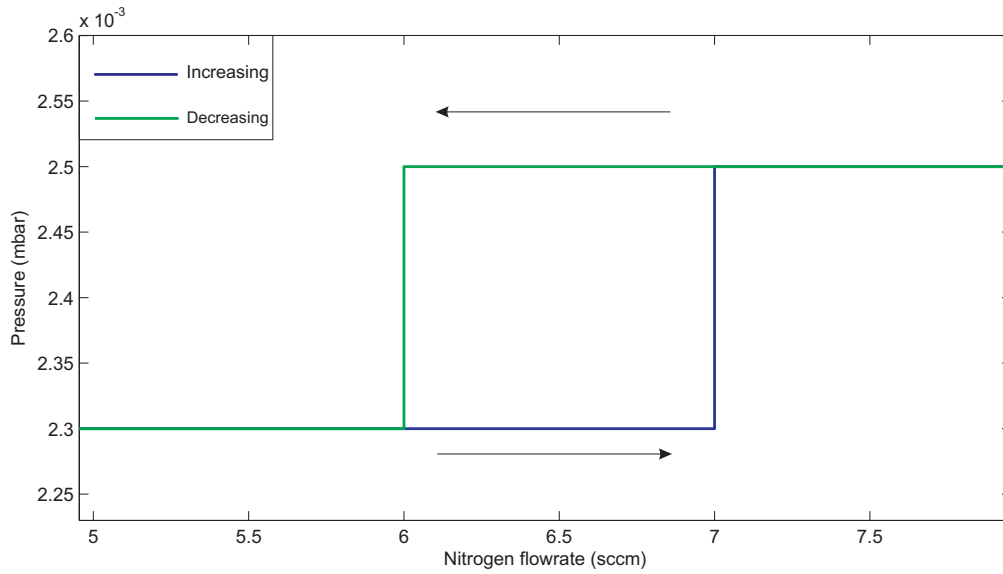Figure 4.6: Hysterisis effect as a function of plasma power

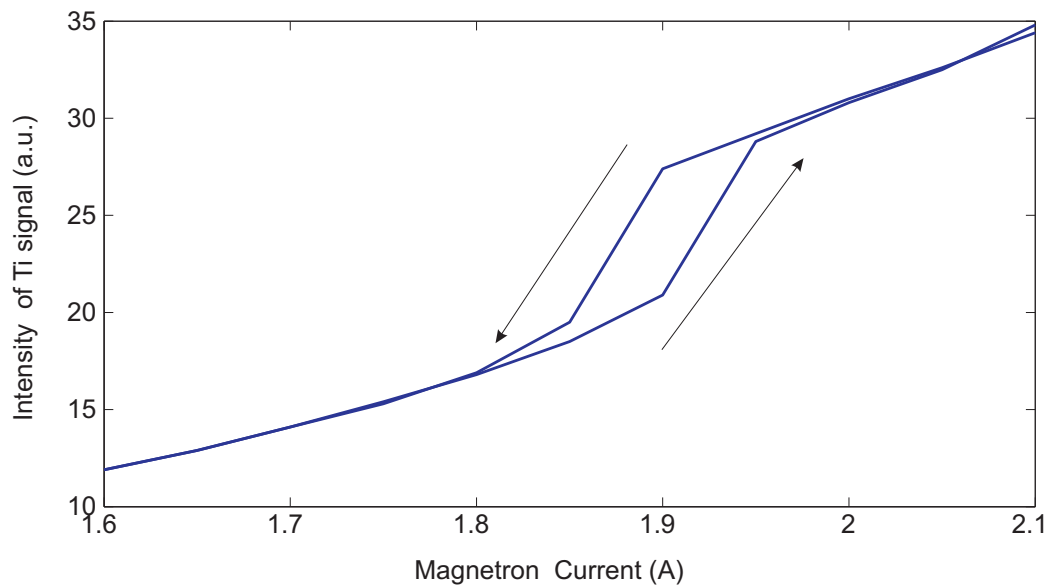Figure 4.7: Hysterisis effect as a function of nitrogen flow rate

Figure 4.8: Hysterisis effect as a function of plasma current

4.4.1 Minimizing the hysteresis area

As explained earlier the hysteresis effect seen in reactive sputtering is the main issue that has to be taken into account if reproducibility is of critical concern. In order to decrease the width of the hysteresis area we increase the Ar flow rate from 40 sccm to 80 sccm while the nitrogen flow rate is kept constant at 4 sccm.As shown in (Figure 4.9) the hysteresis area is dramatically decreased with increasing Ar flow rate and keeping the throttle valve fully open. In order to quantify the hysteresis area, the area under the both
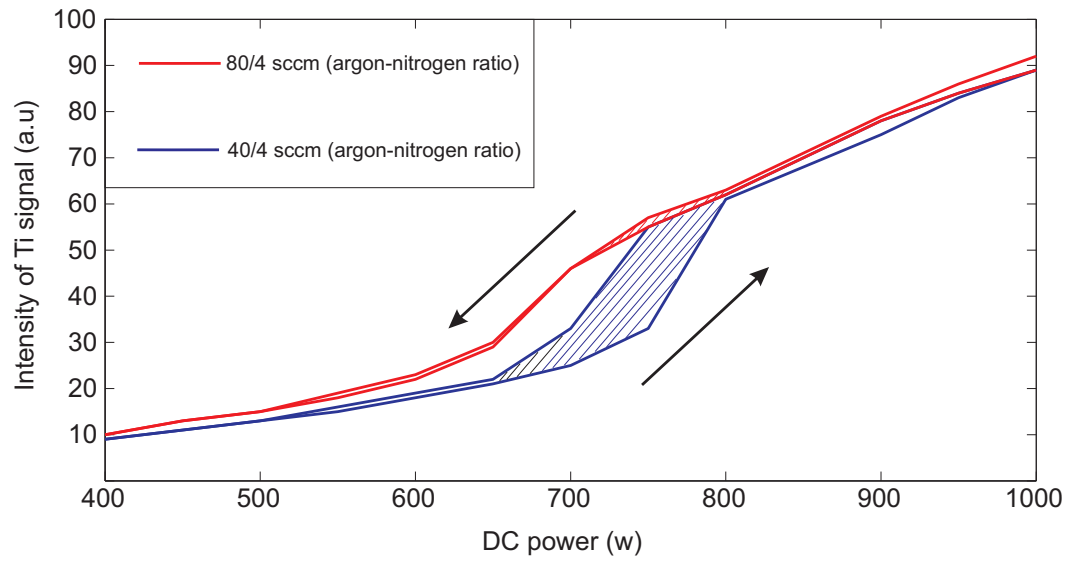
Figure 4.9: Hysteresis effect as function power with different gas mixture ratio

increasing and decreasing curves is calculated based on trapezoid rule and subtracted from each other. The result is shown in (Figure 4.10). This is in agreement with T.Larsson et al. where the hysteresis area is decreased by increasing the pumping speed [22].
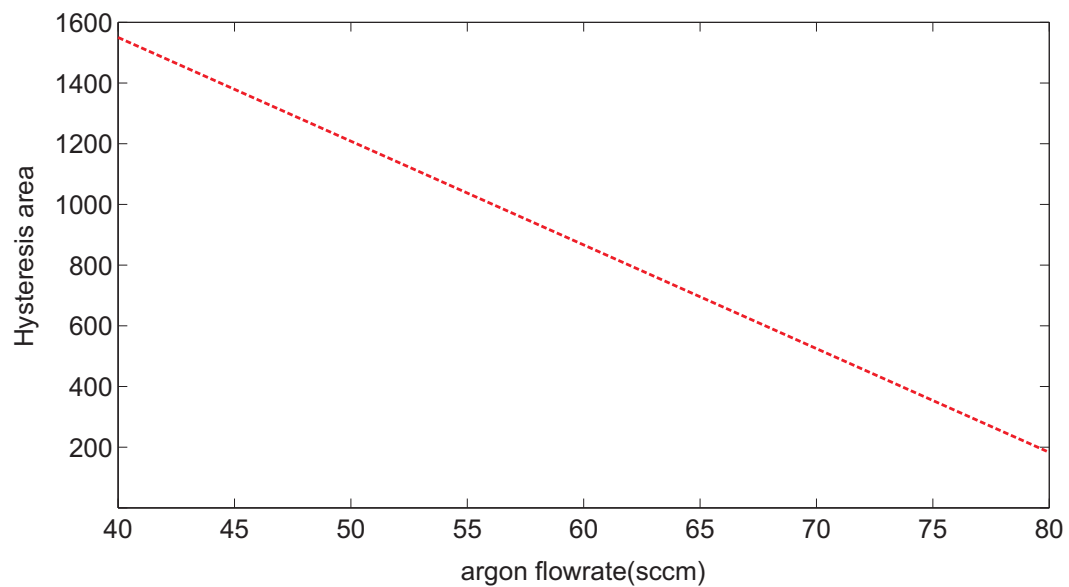

Figure 4.10: Hysteresis area as a function of argon flow rate calculated by trapezoid rule

4.5 Characterization and evaluation of sputtered TiN film at different plasma current

These results are also briefly presented in paper B. Firstly,the plasma emission of the Ti signal as a function of magnetron current was used to detect the stoichiometric TiN which transpires at different Ti peak intensities at ascending and descending magnetron current, by color inspection (Figure 4.11).
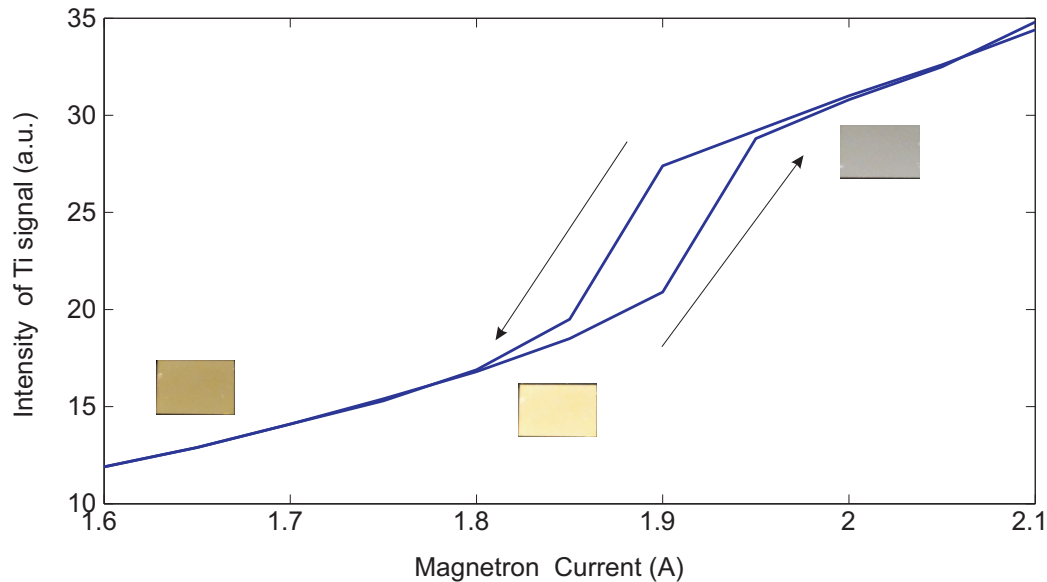

Figure 4.11: Color variation of TiN film at different magnetron currents

Secondly, at different points for the magnetron current ranging from 1.75 A to 2.1 A TiN films were deposited on SiO_2 substrates following by resistivity measurements with the four-point-probe technique. The resistivity results are shown in (Figure 4.12).

As can be clearly seen in (Figure 4.12) the resistivity of the TiN film reaches to a minimum at the same magnetron current yields the stoichiometric TiN film (Figure 4.11). This result is in agreement with the properties of stoichiometric TiN. Furthermore, as can be observed in (Figure 4.13) there is a decrease in the deposition rate when it approaches to the optimum point indicating the formation of stoichiometric TiN on the target surface. In order to investigate the stoichiometry of the optimum point obtained from the previous experiment. XPS analysis was carried out on the sample produced at 1,9 A magnetron current (minimum resistivity). Figure 4.14 shows the the Ti 2p core level photoemission spectrum from unoptimized TiN film and optimized TiN as sputtered by this new method after 5 ion etching to remove the oxide layer on the surface. Clearly a shift appearers between unoptimized and optimized sputtered TiN films. M.Delfino et al. explain this phenomenon in terms of phase change between hcp to fcc TiN where the Ti $2P_{3/2}$ of hcp Ti metal is 453 eV while for stoichiometric TiN (fcc) it is 454.8 eV. It is also claimed that upon the formation of this phase no further change in TiN phases is seen as the nitrogen flow rate increases
[16].

Finally, the diffusion barrier performance of the optimized TiN film was also investigated where the samples were heated up to 650°C with a 100°C per minute ramp rate. As it can be seen in (Figure 4.15)
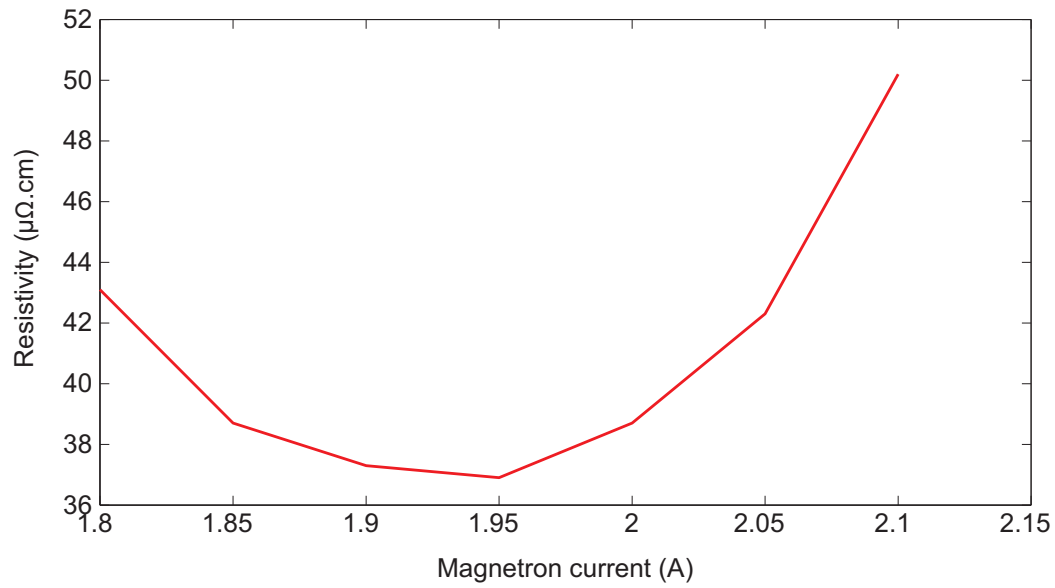
Figure 4.12: Resistivity of TiN film at different point for plasma current

even with 5 nm thick Ni seeds there is no significant diffusion of Ni into the optimized TiN and as a result the VACNFs growth can be initiated.
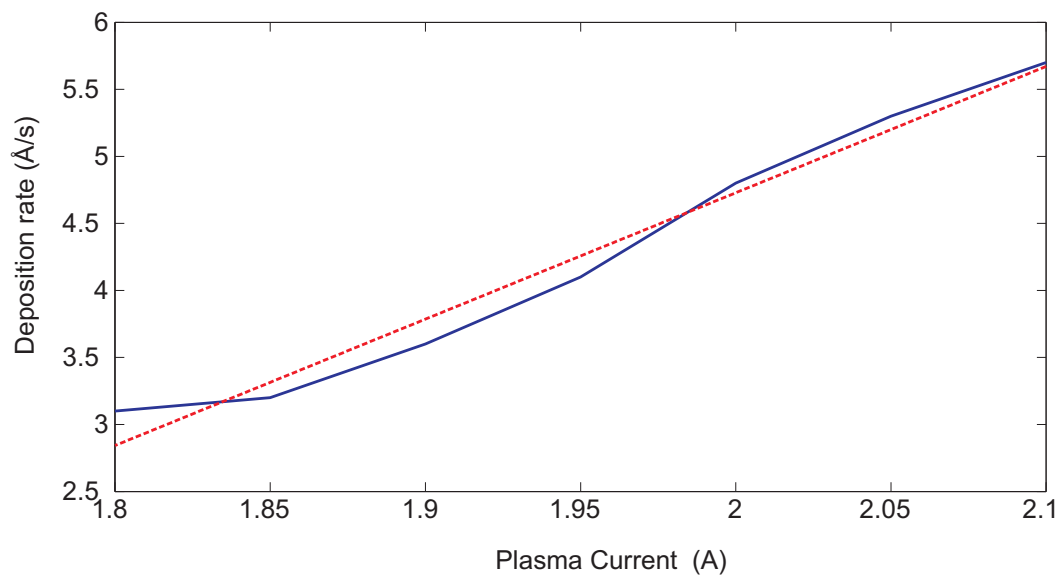

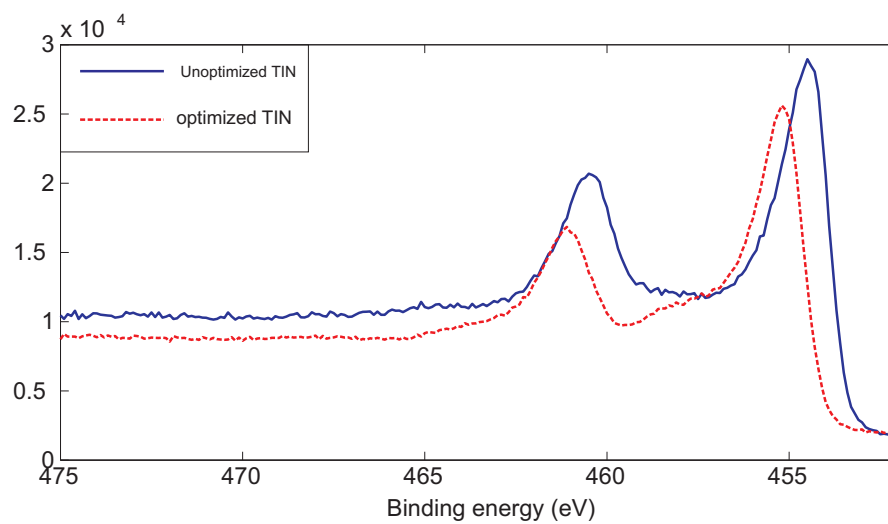Figure 4.13: Deposition rate of TiN versus plasma current

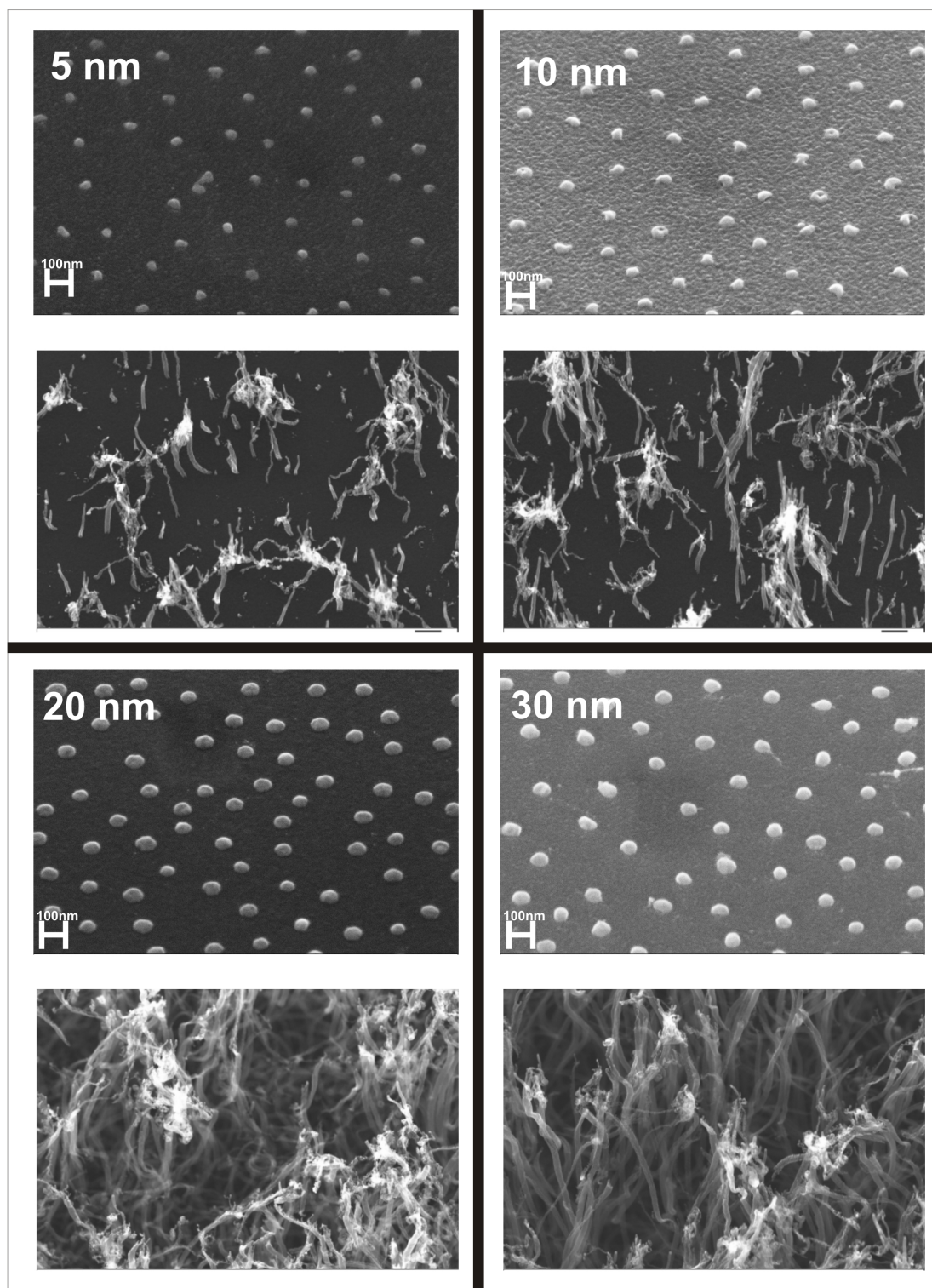Figure 4.14: A comparison between the XPS spectra of optimized and unoptimized TiN

Figure 4.15: Optimized TiN substrate annealing and corresponding VACNFs growth on top of it with different thickness of Ni catalyst seeds

5 Conclusion

We have developed a novel method for producing stoichiometric TiN by dc magnetron reactive sputtering based on monitoring Ti signal intensity while adjusting the magnetron current. We obtained a minimum electrical resistivity of $37\mu\Omega$.cm by employing the substrate plasma during the film deposition. We have shown that the minimum in resistivity is acheived as stoichiometric TiN is formed which is in agreement with previous works [6]. The formation of stoichiometric TiN has also been confirmed by XPS analysis where a shift in binding energy of Ti appeared between the TiN phases. It has also been demonstrated that further change in nitrogen partial pressure does not affect the composition ratio of the film. We have also successfully minimized the diffusion of Ni dots into TiN even at elevated temperatures.

Bibliography

[1] "Pentaheptite allotropes of carbon nanotubes," *ECS Transactions*, vol. 6, no. c, pp. 41–46, 2007.

[2] Farzan Alavian Ghavanini, *Toward Carbon based NEMS With an emphasis on vertically aligned carbon nanofibers*. Göteborg: Chalmers University of Technology, 2009.

[3] TENG WANG, *Twords Carbon Nanotube-based off-Chip Interconnects*. Göteborg: Chalmers re-proservice, 2009.

[4] a. V. Melechko, V. I. Merkulov, T. E. McKnight, M. A. Guillorn, K. L. Klein, D. H. Lowndes, and M. L. Simpson, "Vertically aligned carbon nanofibers and related structures: Controlled synthesis and directed assembly," *Journal of Applied Physics*, vol. 97, no. 4, p. 041301, 2005.

[5] Wolfgang Bacsa, "Who discovered carbon nanotubes?."

[6] J. Sundgren, B. Johansson, S. Karlsson, and H. Hentzell, "Mechanisms of reactive sputtering of titanium nitride and titanium carbide II: Morphology and structure2," *Thin Solid Films*, vol. 105, pp. 367–384, July 1983.

[7] M. Hibbs, J. Sundgren, B. Jacobson, and B. Johansson, "The microstructure of reactively sputtered Ti-N films," *Thin Solid Films*, vol. 107, no. 2, pp. 149–157, 1983.

[8] P. Roquiny, F. Bodart, and G. Terwagne, "Colour control of titanium nitride coatings produced by reactive magnetron sputtering at temperature less than 100 C," *Surface and Coatings Technology*, vol. 116, pp. 278–283, 1999.

[9] R. C. Ellwanger and J. M. Towner, "Thin Solid Films, 161 (1988) 289-304," vol. 161, pp. 289–304, 1988.

[10] H. Melchior, "397 A P P L I C A T I O N S O F TiN T H I N F I L M S I N S I L I C O N D E V I C E TECHNOLOGY*," vol. 93, pp. 397–405, 1982.

[11] Milton Ohring, *Materials Science of Thin Films*. Harbor Drive, Orlando, Florida: Academic Press, second edi ed., 2002.

[12] S. Berg, "Modeling of reactive sputtering of compound materials," *Journal of Vacuum Science & Technology A: Vacuum, Surfaces, and Films*, vol. 5, p. 202, Mar. 1987.

[13] J. Schulte, "Magnetron sputtering of aluminium using oxygen or nitrogen as reactive gas," *Thin Solid Films*, vol. 324, pp. 19–24, July 1998.

[14] F. S.Zhu, "No Title," *international joutnal of materials and product technology*, p. 101, 2001.

[15] J. Musil, S. Kadlec, and V. Valvoda, "107 NEW RESULTS IN d.c. REACTIVE TiN, FILMS*," *October*, vol. 167, 1988.

[16] M. Delfino, J. A. Fair, and D. Hodul, "X-ray photoemission spectra of reactively sputtered TiN," *Journal of Applied Physics*, vol. 71, no. 12, p. 6079, 1992.

[17] F. M. SMITS, "Measurement of sheet resistivities with the four point prose.pdf," *The bell system technical journal*, vol. 37, pp. 711–718, 1958.

[18] B.-O. J. J.-E. SUNDGREN and S.-E. KARLSSON, "INFLUENCE OF PROCESS PARAMETERS ON FILM COMPOSITION1," *Thin Solid Films*, vol. 105, pp. 353–366, 1983.

[19] V. Kirchhoff and U. Heisig, "Control of reactive d.c. magnetron sputtering of SnO2 by means of optical emission," *Surface and Coatings Technology*, vol. 59, pp. 101–104, Oct. 1993.

[20] T. Nyberg, S. Berg, U. Helmersson, and K. Hartig, "Eliminating the hysteresis effect for reactive sputtering processes," *Applied Physics Letters*, vol. 86, no. 16, p. 164106, 2005.

[21] Ajay Kurnar Arora & Abhai Mansingh, "EFFECT OF TARGET SUBSRATE DISL;WCE CM THE PRDPERITFS OF RF SPUTTERED PZT FILMS," *Physical Review*, pp. 4–6.

[22] T. Larsson, "A physical model for eliminating instabilities in reactive sputtering," *Journal of Vacuum Science & Technology A: Vacuum, Surfaces, and Films*, vol. 6, p. 1832, May 1988.